Manganese-Rich Sandstones as an Indicator of Ancient Oxic Lake Water Conditions in Gale Crater, Mars

P. Gasda, N. Lanza, P.-y. Meslin, S. Lamm, A. Cousin, R. Anderson, O. Forni, E. Swanner, J. L'haridon, J. Frydenvang, et al.

JGR Planets

RESEARCH ARTICLE

10.1029/2023JE007923

Manganese-Rich Sandstones as an Indicator of Ancient Oxic Lake Water Conditions in Gale Crater, Mars

P. J. Gasda[1], N. L. Lanza[1], P.-Y. Meslin[2], S. N. Lamm[3], A. Cousin[2], R. Anderson[4], O. Forni[2], E. Swanner[5], J. L'Haridon[6], J. Frydenvang[7], N. Thomas[8], S. Gwizd[9], N. Stein[8], W. W. Fischer[8], J. Hurowitz[10], D. Sumner[11], F. Rivera-Hernández[12], L. Crossey[13], A. Ollila[1], A. Essunfeld[1], H. E. Newsom[13], B. Clark[14], R. C. Wiens[15], O. Gasnault[2], S. M. Clegg[1], S. Maurice[2], D. Delapp[1], and A. Reyes-Newell[1]

[1]Los Alamos National Laboratory, Los Alamos, NM, USA, [2]Institut de Recherche en Astrophysique et Planétologie, Universite de Toulouse, CNRS, CNES, UPS, Toulouse, France, [3]University of Kansas, Lawrence, KS, USA, [4]U.S. Geological Survey Astrogeology Science Center Flagstaff, Flagstaff, AZ, USA, [5]Iowa State University, Ames, IA, USA, [6]European Science Foundation, Strasbourg, France, [7]University of Copenhagen, Copenhagen, Denmark, [8]California Institute of Technology, Pasadena, CA, USA, [9]Jet Propulsion Laboratory, Pasadena, CA, USA, [10]Stony Brook University, Stony Brook, NY, USA, [11]University of California Davis, Davis, CA, USA, [12]Georgia Institute of Technology, Atlanta, GA, USA, [13]The University of New Mexico, Albuquerque, NM, USA, [14]Space Science Institute, Boulder, CO, USA, [15]Earth, Atmospheric, and Planetary Sciences, Purdue University, West Lafayette, IN, USA

Abstract Manganese has been observed on Mars by the NASA *Curiosity* rover in a variety of contexts and is an important indicator of redox processes in hydrologic systems on Earth. Within the Murray formation, an ancient primarily fine-grained lacustrine sedimentary deposit in Gale crater, Mars, have observed up to 45× enrichment in manganese and up to 1.5× enrichment in iron within coarser grained bedrock targets compared to the mean Murray sediment composition. This enrichment in manganese coincides with the transition between two stratigraphic units within the Murray: Sutton Island, interpreted as a lake margin environment, and Blunts Point, interpreted as a lake environment. On Earth, lacustrine environments are common locations of manganese precipitation due to highly oxidizing conditions in the lakes. Here, we explore three mechanisms for ferromanganese oxide precipitation at this location: authigenic precipitation from lake water along a lake shore, authigenic precipitation from reduced groundwater discharging through porous sands along a lake shore, and early diagenetic precipitation from groundwater through porous sands. All three scenarios require highly oxidizing conditions and we discuss oxidants that may be responsible for the oxidation and precipitation of manganese oxides. This work has important implications for the habitability of Mars to microbes that could have used Mn redox reactions, owing to its multiple redox states, as an energy source for metabolism.

Plain Language Summary In May 2017, the NASA *Curiosity* rover observed higher than usual amounts of manganese in the lakebed rocks within Gale crater, Mars. These sedimentary rocks have larger grain sizes than what is typical for the lakebed rocks in Gale crater. This may indicate that the original sediments were formed in a river, delta, or near the shoreline in the ancient lake. In this paper, we discuss how manganese could have been enriched in these rocks—for example, by percolation of groundwater through the original sediments or through the rock afterward—and what oxidant could be responsible for the precipitation of manganese in the rocks. On Earth, manganese becomes enriched because of oxygen in the atmosphere and this process is often sped up by the presence of microbes. Microbes on Earth can use the many oxidation states of manganese as energy for metabolism; if life was present on ancient Mars, the increased amounts of manganese in these rocks along the lake shore would be a helpful energy source for life.

Key Points:

- Enrichments of MnO are observed in bedrock and diagenetic features near a stratigraphic boundary between possible lake margin and lake sediments
- Manganese precipitation may have occurred along a lake shoreline via authigenic or early diagenetic scenarios
- All alteration scenarios require persistent water and highly oxidizing conditions in what would have been a habitable environment

Supporting Information:

Supporting Information may be found in the online version of this article.

Correspondence to:

P. J. Gasda,
gasda@lanl.gov

Citation:

Gasda, P. J., Lanza, N. L., Meslin, P.-Y., Lamm, S. N., Cousin, A., Anderson, R., et al. (2024). Manganese-rich sandstones as an indicator of ancient oxic lake water conditions in Gale crater, Mars. *Journal of Geophysical Research: Planets*, *129*, e2023JE007923. https://doi.org/10.1029/2023JE007923

Received 23 MAY 2023
Accepted 27 MAR 2024

Author Contributions:

Conceptualization: P. J. Gasda, N. L. Lanza, P.-Y. Meslin, A. Cousin, E. Swanner, J. Frydenvang, N. Stein, W. W. Fischer, J. Hurowitz, D. Sumner, F. Rivera-Hernández, L. Crossey, H. E. Newsom, B. Clark, R. C. Wiens, O. Gasnault, S. M. Clegg, S. Maurice
Data curation: J. Frydenvang, F. Rivera-Hernández, A. Essunfeld, D. Delapp, A. Reyes-Newell

1. Introduction

Recent observations of manganese precipitation in rocks on Mars by the NASA Mars Science Laboratory *Curiosity* and Mars Exploration Rover *Opportunity* rovers (Arvidson et al., 2016; Berger et al., 2020, 2022; Gasda et al., 2022; Lanza et al., 2014, 2016, 2022; Meslin et al., 2018; Thompson et al., 2020; Treiman et al., 2023) and in martian meteorites (Cao et al., 2018; Liu et al., 2017, 2021; Nakamura et al., 2023) raise important questions about the range of redox conditions that have existed within martian environments and how they have changed over time. Since manganese-rich materials were first observed in Gale crater (Lanza et al., 2014), sediments containing abundant MnO have been observed periodically throughout the *Curiosity* rover's traverse in a range of

Formal analysis: P. J. Gasda, N. L. Lanza, P.-Y. Meslin, S. N. Lamm, A. Cousin, R. Anderson, O. Forni, J. L'Haridon, J. Frydenvang, N. Thomas, S. Gwizd, N. Stein, W. W. Fischer, F. Rivera-Hernández, A. Ollila, A. Essunfeld, S. M. Clegg
Funding acquisition: R. C. Wiens, O. Gasnault, S. M. Clegg, S. Maurice
Investigation: P. J. Gasda, N. L. Lanza, P.-Y. Meslin, S. N. Lamm, A. Cousin, J. L'Haridon, J. Frydenvang, N. Thomas, A. Ollila, S. M. Clegg, A. Reyes-Newell
Methodology: P. J. Gasda, A. Cousin, R. Anderson, O. Forni, J. Frydenvang, N. Thomas, N. Stein, W. W. Fischer, J. Hurowitz, F. Rivera-Hernández, A. Ollila, S. M. Clegg, S. Maurice
Project administration: N. L. Lanza, R. C. Wiens, O. Gasnault, S. M. Clegg, S. Maurice
Resources: N. L. Lanza, R. C. Wiens, O. Gasnault, S. M. Clegg, S. Maurice
Software: A. Cousin, R. Anderson, O. Forni, N. Thomas, L. Crossey, A. Essunfeld, D. Delapp
Supervision: N. L. Lanza, R. C. Wiens, O. Gasnault, S. M. Clegg, S. Maurice
Validation: A. Cousin, R. Anderson, O. Forni, N. Thomas, F. Rivera-Hernández, S. M. Clegg
Visualization: P. J. Gasda, L. Crossey, A. Essunfeld
Writing – original draft: P. J. Gasda, N. L. Lanza, P.-Y. Meslin, A. Cousin, R. Anderson, E. Swanner, J. Frydenvang, N. Thomas, N. Stein, W. W. Fischer, D. Sumner, F. Rivera-Hernández, L. Crossey, A. Ollila, H. E. Newsom, B. Clark, R. C. Wiens, O. Gasnault, S. M. Clegg, S. Maurice
Writing – review & editing: P. J. Gasda, N. L. Lanza, P.-Y. Meslin, A. Cousin, R. Anderson, E. Swanner, J. Frydenvang, S. Gwizd, W. W. Fischer, J. Hurowitz, F. Rivera-Hernández, L. Crossey, A. Ollila, A. Essunfeld, H. E. Newsom, B. Clark, R. C. Wiens, O. Gasnault, S. M. Clegg, S. Maurice

geologic contexts (Frydenvang et al., 2020; Gasda et al., 2022; Lanza et al., 2016, 2022; L'Haridon et al., 2018, 2020; Meslin et al., 2018; Sun et al., 2019). The presence of Mn-bearing precipitates likely indicates varying past redox and pH conditions on Mars. On Earth, manganese precipitation from water is one of several key indicators for a major global shift in redox conditions brought about by the rise in atmospheric O_2 by photosynthetic life during the Great Oxygenation Event ~2.3 Ga (GOE; Anbar & Holland, 1992; Kirschvink et al., 2000; Klemm, 2000; Schissel & Aro, 1992; Tsikos et al., 2003; Ostrander et al., 2019). Because the kinetics of Mn(II) oxidation by oxygen are sluggish at neutral pH, it is thought that most manganese cycling on Earth is catalyzed by microbes (e.g., Aller, 1994; Hansel, 2017; Kristensen et al., 2003; Tebo et al., 2004; Yu & Leadbetter, 2020). The mechanism of manganese precipitation on Mars is likely abiotic but raises intriguing questions about its habitability and potential biosignatures on Mars. The observation of manganese-bearing precipitates on Mars highlights the possibility that modes of high-potential redox chemistry were present on Mars. Because high valent Mn species are themselves powerful oxidants (Stumm & Morgan, 1996), their presence on Mars could have transformed additional inorganic or organic species present and the planet's geology overall.

The timing and geologic context for manganese precipitation in the Gale crater is complex and appears to be the result of multiple processes. Manganese abundance along the *Curiosity* rover's traverse has shown considerable variation within sedimentary rocks and veins, ranging from below ChemCam's detection limit of 27 ppm up to 22 wt% MnO in localized (mm to cm) areas (Frydenvang et al., 2020; Gasda et al., 2021, 2022; Lanza et al., 2014, 2016; Treiman et al., 2023). Note that a recent ChemCam calibration for MnO (Gasda et al., 2021) has revised, and generally decreased the compositions reported earlier. These new quantifications are available from the Planetary Data System (PDS) (Wiens, 2021a, 2021b). Some instances of Mn precipitation clearly post-date the lithification of the sediments—including coatings (Lanza et al., 2015) and fracture fills (Lanza et al., 2016). Other instances of elevated MnO precipitation may have accumulated during early diagenesis of the lake sediments within concretions (Gasda et al., 2022; Lanza et al., 2022; L'Haridon et al., 2018; Meslin et al., 2018; Sun et al., 2019; Treiman et al., 2023). On the other hand, many high MnO observations present in sedimentary rocks do not fit either model. Thus, it is an open question whether some instances of elevated Mn abundance in Gale were formed authigenically, diagenetically, or by some combination of the two. Here we report Mn precipitation within deltaic/lacustrine sandstones within Gale crater lacustrine sediments that suggests a syn-depositional timing for sedimentation and Mn precipitation. Based on the hypothesis that the Gale lake was redox stratified (Hurowitz et al., 2017), we suggest an additional mechanism for Mn precipitation that is similar to what is observed in terrestrial redox-stratified lakes.

Within typical Murray formation (hereafter simply "Murray") bedrock, which is the primarily fine-grained layered lacustrine sediment within Gale crater (e.g., Vasavada, 2022), the median manganese abundance is ~0.08 wt% MnO. This low Mount Sharp group composition for MnO likely reflects early chemical alteration of the Murray bedrock to produce phyllosilicates under alkaline and reducing (with respect to Mn oxide formation) and low pCO_2 (partial pressure of CO_2) conditions (e.g., Turner et al., 2021). Relatively anoxic groundwater conditions likely would draw out Mn^{2+} from the primary bedrock where Mn^{2+} would remain in the groundwater if Mn^{2+} remains dilute and if pCO_2 remains low in the groundwater (e.g., Berger et al., 2022; Gasda et al., 2022). Geochemical models of the alteration mineral assemblage for Murray do not tend to predict major amounts of Mn-bearing phases, and the trace amounts that are predicted for models are reduced phases (Turner et al., 2021). *Curiosity* ChemCam data reported here can only account for total Mn oxide abundance and cannot directly measure Mn speciation. Although Murray bedrock typically contains low MnO abundance, a large increase in MnO abundance was observed in the Murray formation between Mars solar days (Sol) 1685 and 1689 near −4,280 m elevation (Figure 1). The increased concentration of MnO in the bedrock coincides with a transition between two stratigraphic members of the Murray, "Sutton Island" and "Blunts Point" (Figure 1). The increase in MnO abundance also coincides with coarser-grained bedrock that is also part of the Murray formation (Figure 1; Rivera-Hernández et al., 2020). This large sharp increase of MnO within a particular bedrock facies (described later) coincides with a steady increase of MnO in the bedrock to the transition, and a steady decrease thereafter (Figure 1). The high concentration of MnO observed in this area is similar in abundance to previous observations of groundwater-precipitated MnO that were interpreted as fracture fills (Lanza et al., 2014, 2016) and diagenetic features observed in "Glen Torridon" (Gasda et al., 2022; Treiman et al., 2023). However, high manganese abundances are not consistently associated with the diagenetic features that are also present in these local strata, for example, fracture filling veins and concretions (e.g., L'Haridon et al., 2018; Meslin et al., 2018; Sun et al., 2019). Veins are indicators of late-stage diagenesis due to groundwater alteration that occurred post-

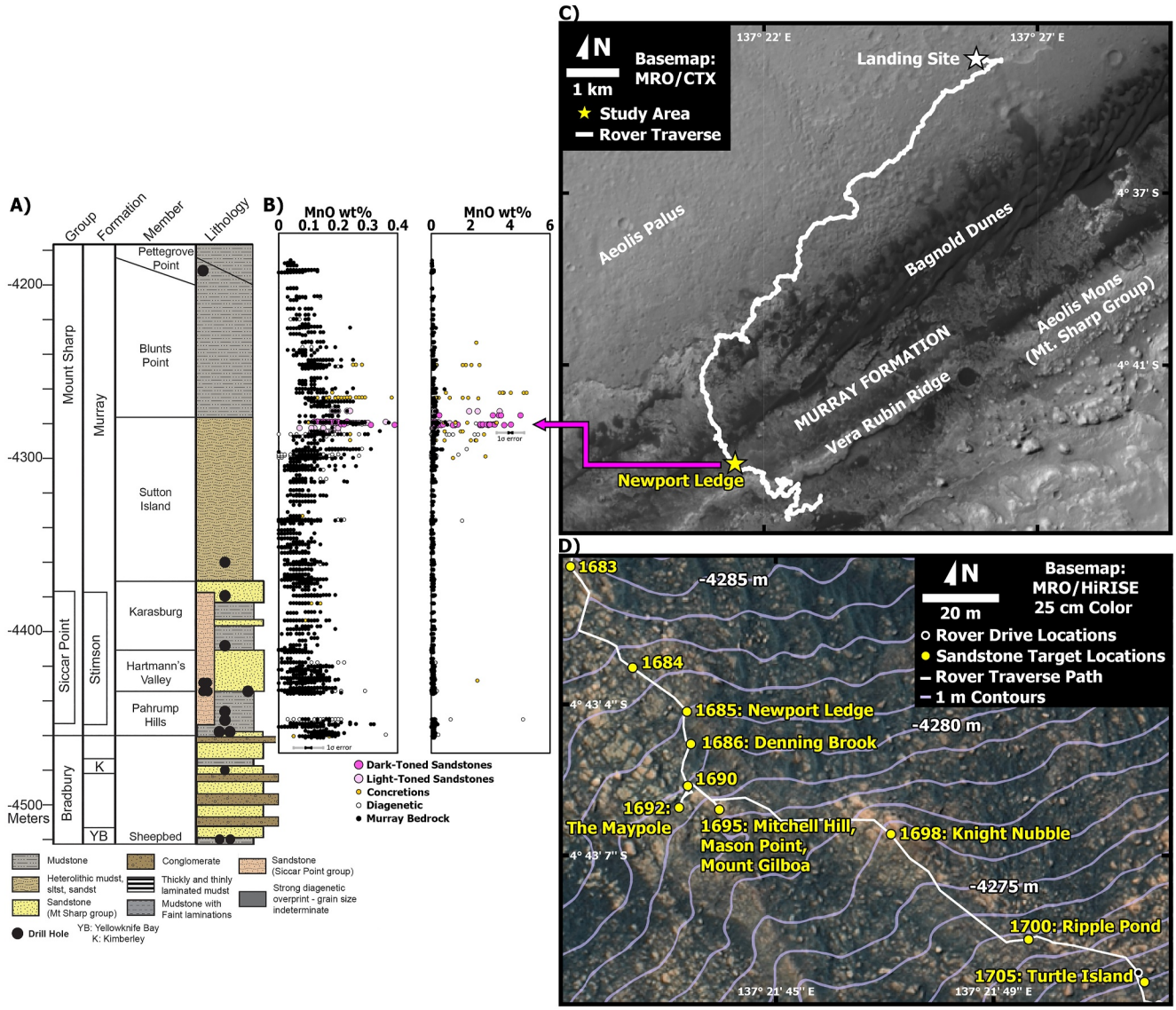

Figure 1. (a) The chemostratigraphic representation is a record of the rover's climb through the Bradbury, Mount Sharp, and Siccar Point Group (the stratigraphic column was prepared by Mars Science Laboratory Sedimentology and Stratigraphy Working Group), focusing on the Murray formation below Vera Rubin ridge, with (b) MnO abundance versus elevation relative to mean Mars elevation. A plot expanding the range of bedrock compositions (≤0.4 wt% MnO) is shown on the left, and the full range of MnO (up to 6 wt% MnO) is shown on the right. Calcium sulfate and high-silica diagenetic features have been removed. Major facies plotted: Murray bedrock (black), diagenetic features (white), diagenetic concretions (orange), dark-toned sandstones (magenta), and light-toned sandstones (pink). Both plots in panel (b) show the same data. (c) The location of Newport Ledge is labeled along the traverse and the pink arrow shows this location on the MnO versus. elevation plot. (d) The locations with high manganese sandstones are shown on the traverse map with 1 m contour lines. The AEGIS post drive targets listed in Table 1 occurred on the corresponding labeled sol locations.

lithification and fracturing of the bedrock. Some of the nodular diagenetic features, some of which can have high MnO, appear to have formed during an early diagenetic event (Meslin et al., 2018).

Authigenic manganese cycling and precipitation within a redox-stratified lake have been hypothesized for Gale crater (Hurowitz et al., 2017). Observations of two distinct mineral facies that are juxtaposed in the Pahrump Hills member of the Murray formation suggest that redox conditions varied within the lake. One facies consists of magnetite-silica bearing materials (MS), which imply a less oxidizing environment, and the other facies consists of hematite-phyllosilicate bearing materials (HP) that required more oxidizing conditions to form. Within the stratigraphic column—up to sol 1300, the last data reported in that work—the MS facies appears sandwiched between two occurrences of the HP facies at Pahrump Hills, a chemically unique location within the Murray.

Notably, the oxidized HP facies are also associated with higher abundances of Mn. In the study area of this work, MS facies have not been encountered in the stratigraphy; however, the *Curiosity* drill capability was offline between sols ∼1500–2050 and the mission did not have a way to confirm the mineralogy. Hurowitz et al. (2017) suggested that the observed mineral facies may be explained by depth-dependent variations in dissolved atmospheric oxidants and other dissolved solutes. With this model in mind, we explore the hypothesis that the observed Mn-bearing precipitates in this section of the *Curiosity* traverse may be authigenic (i.e., syn-depositional, precipitated within lake sediments from water) or an early diagenetic product, and that they formed in shallow, oxygenated waters. Here, we examine stratigraphy, sedimentology, and chemistry to constrain the environmental conditions and processes by which manganese could have been concentrated within Murray sediments.

1.1. Geologic Context

Gale is a ∼152 km wide crater situated on the edge of the Mars Southern Highlands, Northern Lowlands dichotomy. Gale's central mound, Aeolis Mons (informally "Mount Sharp"), rises 5 km above the crater floor, Aeolis Palus, and is largely comprised of sedimentary rocks (Fraeman et al., 2016; Malin & Edgett, 2000; Milliken et al., 2010). Gale is interpreted as having hosted a habitable redox-stratified lake or series of lakes in its past based on chemical, mineral, and stratigraphic evidence of hematite and phyllosilicate-bearing fluvial-deltaic deposits and lacustrine mudstones (Edgar et al., 2020; Grotzinger et al., 2014, 2015; Gwizd et al., 2022, 2023; Hurowitz et al., 2017; Vaniman et al., 2014). The Gale lake produced 100s of meters of typically fine-grained thinly laminated lake sediment deposits, collectively named the Murray formation (Edgar et al., 2020; Rivera-Hernández et al., 2020).

The Murray formation is comprised of seven members of primarily mudstone and some coarser grained strata (Vasavada, 2022). Here, we focus on the strata in the Murray formation below Vera Rubin ridge (VRR), where abundances of the major oxides in the bedrock, including FeO_T and CaO, do not vary greatly over the stratigraphic section, but MnO and MgO do vary (Frydenvang et al., 2020). The first member encountered by the rover was Pahrump Hills, which is interpreted as mainly a fine-grained layered mudstone lacustrine deposit (Edgar et al., 2020; Fedo et al., 2017, 2018; Grotzinger et al., 2015; Gwizd et al., 2022, 2023; Rivera-Hernández et al., 2019, 2020; Stack et al., 2019). The Hartmann's Valley and Karasberg deposits are interpreted as a mix of lake and lake margins and potentially aeolian deposits (Gwizd et al., 2022). The Sutton Island member is characterized by a "heterolithic texture" and is interpreted as possibly a deltaic lake margin (Edgar et al., 2020; Fedo et al., 2017, 2018; Gwizd et al., 2022, 2023), with many indications of drying—mudcracks (Stein et al., 2018), high salinity intervals, and enrichment of highly soluble elements in the bedrock and veins (Achilles et al., 2020; Das et al., 2020; Gasda et al., 2017; Rapin et al., 2019; Thomas et al., 2019). Above Sutton Island, there is a return to a lacustrine setting with finely layered mudstone in the Blunts Point member. The major element oxide chemostratigraphy of the Murray formation bedrock varies little below VRR and above the Pahrump Hills (Frydenvang et al., 2020). Manganese composition of the bedrock also remains approximately constant, with slight variations between Pahrump Hills and −4,320 m elevation (the mid-way point through the Sutton Island Member) before increasing to much higher levels at the Sutton Island to Blunts Point transition (Figure 1). Manganese enrichment in diagenetic features are quite rare in the Murray formation below approximately −4,300 m in elevation, are common in the Sutton Island to Blunts Point region, and are absent at higher elevations. In terms of diagenetic features, lower elevations of Murray are dominated by calcium sulfate veins (Das et al., 2020; Gasda et al., 2017; Kronyak et al., 2019; L'Haridon et al., 2018, 2020; Nachon et al., 2014, 2017; Rapin et al., 2016; Schwenzer et al., 2016), and concretions, dark layers, and other features occur at specific locations along the traverse within the Murray (David et al., 2020; Gasda et al., 2022; Meslin et al., 2018; Sun et al., 2019).

2. Methods

Microscale manganese abundances were measured using ChemCam—an atomic emission spectroscopy instrument that uses laser-induced breakdown spectroscopy (LIBS) to quantify elemental abundances present in a target. The ChemCam LIBS uses a pulsed laser emitting a 1,067 nm beam that is focused onto a target up to 7 m from the rover, which produces an analytical footprint of 350–550 μm (Maurice et al., 2012; Wiens et al., 2012). Each laser pulse ablates and ionizes a small (∼nanograms to micrograms) amount of material. Light emitted from the plasma formed by each laser pulse is collected by the ChemCam telescope, and spectra are recorded by the ultraviolet, violet, and visible to near infrared spectrometers. Hence, each laser shot provides a spectrum with

6,144 channels; 30 shots are typically recorded per observation point, with the last 25 shots averaged to avoid the surficial dust signature in the first 5 shots (Lasue et al., 2018). For each target, the laser analyzes multiple points across the surface in a line or grid, called a "raster," to record a representative chemistry for a target. The instrument's Remote Micro Imager (RMI) records an image before and after each LIBS raster to provide the geological context for each target (Le Mouélic et al., 2015). Major element oxide chemistry is determined from the LIBS spectrum using a multivariate calibration model trained on >400 rock powder standards (Clegg et al., 2017; Wiens et al., 2013), and manganese oxide abundance is determined from a multivariate model using additional standards to specifically address the range of Mn abundance expected for Mars and improve accuracy of the Mn calibration model for targets on Mars (Gasda et al., 2021). A preliminary SO_3 calibration is used in this work (Clegg et al., 2020). The average SO_3 compositions for each target reported here (Table 1) are within ~1 wt% of those reported by the Alpha Particle X-ray Spectrometer (APXS; Campbell et al., 2014) instrument on the same targets (Berger et al., 2020; see Supplementary Text S1). Elements not quantified for ChemCam, for example, P, and Cl, are observed in ChemCam spectra using their diagnostic lines if present above the ChemCam detection limit, and the peak area for the element can be used to determine relative amounts of the element in an observation (Meslin et al., 2018; Thomas et al., 2019). To determine the mean bedrock composition of the Murray formation, and the values given in Table 1, clear diagenetic materials (e.g., veins), soil, or out of focus points were excluded. Mean bedrock compositions also exclude the Mn-rich targets (shown in Figure 1b). A full description of each target and its corresponding Mastcam and RMI imagery are available in the Supplementary Materials.

To fully understand the context for ChemCam chemistry and image data, we also examined images from Mastcam (Malin et al., 2010) and the Mars Hand Lens Imager (MAHLI) (Edgett et al., 2012, 2015) onboard the *Curiosity* rover.

Targets were investigated for this work based on three criteria: a GINI Index ≥0.1, which indicates coarser grained rocks (Rivera-Hernández et al., 2019); no significant diagenetic alteration (e.g., nodules and veins); and where at least five ChemCam observation points hit bedrock. Bedrock points are determined first by looking at RMI images and confirming that a point was in focus and did not hit a vein or nodule directly. Targets were classified as either "light-toned" or "dark-toned" by examining targets in Mastcam images. Target RMIs were merged with Right Mastcam images and color corrected for white balance to increase contrast to provide the highest resolution color images when appropriate imagery was available. The RMI images enable comparison of the target before and after the laser shots, which remove the dust from the surface of the target. Dark-toned sandstones, although dusty, appear dark-toned in Mastcam images or in places where the dust has been cleared away by ChemCam laser shots. Light-toned sandstones have a color and tone similar to surrounding Murray bedrock; thus, they are relatively lighter toned than the dark-toned sandstones. The GINI Index Mean Score is a proxy for grain size that has been calibrated using analysis of MAHLI images, where a larger GINI Index corresponds to a coarser grained rock (Rivera-Hernández et al., 2019, 2020). The GINI Index uses compositional variability of ChemCam observations within a given target's shot to shot data (25 laser shots per observation point) to estimate the grain size, assuming that the bedrock composition is relatively homogeneous over a full ChemCam raster. Most targets in the Murray formation are mudstone or siltstone; within the Newport Ledge area, 6 out of 15 targets have GINI Index <0.1 or are associated with diagenetic features (Rivera-Hernández et al., 2020). The rest of the targets have a GINI Index ≥0.1, which was chosen as the criterion for this study, corresponding to very fine sand and larger grain sizes.

The APXS instrument also detects an increase in MnO at the Sutton Island to Blunts Point (Berger et al., 2020, 2022; Thompson et al., 2020). There are some minor differences in compositional values between the two instruments; this is likely due in part from the presence of dust on target surfaces but also from differences in spot size, interrogation depth, and uncertainties of the two instruments. With only four APXS-ChemCam cross targets in this area, combined with dust on these targets, it is difficult to compare absolute values for some elements or compare trends between APXS and ChemCam datasets (e.g., Schmidt et al., 2018). Nevertheless, Supplementary Text S1 provides an analysis of the APXS data and the corresponding MAHLI images from these targets using the supplementary data of Berger et al. (2020).

3. Observations Along the Traverse

Manganese enrichment have been observed in the Murray formation primarily in the Sutton Island and Blunts Point members, especially in the coarser grained rocks (Figure 1). Calcium sulfate vein targets, which typically

Journal of Geophysical Research: Planets

10.1029/2023JE007923

Table 1
ChemCam Compositions of Dark- and Light-Toned Sandstone Targets Compared to Mean Sutton Island and Blunts Point Bedrock

Sol		GINI index[a]	$SiO_2 \pm 1\sigma$[b]	$TiO_2 \pm 1\sigma$	$Al_2O_3 \pm 1\sigma$	$FeO_T \pm 1\sigma$	$MgO \pm 1\sigma$	$CaO \pm 1\sigma$	$Na_2O \pm 1\sigma$	$K_2O \pm 1\sigma$	$MnO \pm 1\sigma$	$SO_3 \pm 1\sigma$[c]	H_2O[d]	OxideTotal	N[e]
	Sutton Island Mean Bedrock	**0.05**	**51.10 ± 5.65**	**0.94 ± 0.13**	**11.56 ± 2.05**	**18.61 ± 2.15**	**5.79 ± 2.02**	**3.91 ± 4.62**	**2.50 ± 0.84**	**1.05 ± 0.45**	**0.07 ± 0.05**	**6.50 ± 4.70**	**2.51**	**102.04**	**1513**
	Blunts Point Mean Bedrock	**0.04**	**49.52 ± 6.62**	**0.90 ± 0.14**	**10.91 ± 2.36**	**18.41 ± 2.54**	**5.35 ± 2.31**	**5.76 ± 6.40**	**2.36 ± 1.14**	**1.08 ± 0.47**	**0.10 ± 0.06**	**8.66 ± 6.58**	**2.11**	**103.05**	**792**
	Dark-Toned Sandstones	**0.18**	**47.58 ± 3.44**	**1.04 ± 0.64**	**9.54 ± 2.49**	**21.68 ± 2.60**	**7.17 ± 2.27**	**2.84 ± 1.78**	**2.37 ± 0.48**	**0.54 ± 0.25**	**1.42 ± 1.41**	**6.76 ± 1.96**	**6.94**	**100.94**	**47**
1685	AEGIS post 1685a	0.2	47.61 ± 2.08	1.18 ± 0.76	6.77 ± 1.72	21.21 ± 1.38	5.11 ± 1.08	5.01 ± 1.86	2.07 ± 0.26	0.53 ± 0.10	1.68 ± 1.17	8.23 ± 1.28	7.05	99.39	9
1686	Newport Ledge ccam	n.d.[f]	49.24 ± 2.40	0.94 ± 0.09	7.34 ± 1.28	22.90 ± 0.52	4.22 ± 0.67	1.64 ± 0.65	2.19 ± 0.37	0.32 ± 0.11	2.83 ± 0.24	5.16 ± 0.54	5.33	96.78	5
1689	Denning Brook	0.13	43.32 ± 2.16	0.83 ± 0.14	9.76 ± 0.84	24.71 ± 1.35	9.07 ± 1.35	2.01 ± 0.85	2.73 ± 0.35	0.46 ± 0.16	1.96 ± 1.31	7.29 ± 1.03	11.01	102.14	10
1695	Mason Point ccam	0.17	48.64 ± 2.93	0.83 ± 0.06	10.99 ± 1.25	20.48 ± 0.88	7.58 ± 1.19	1.99 ± 1.01	2.34 ± 0.40	0.66 ± 0.23	0.16 ± 0.02	7.06 ± 0.87	4.10	100.73	9
1695	Mitchell Hill	0.18	50.16 ± 2.68	1.24 ± 1.01	11.32 ± 2.24	18.43 ± 1.43	9.39 ± 1.10	2.61 ± 1.79	2.14 ± 0.37	0.58 ± 0.17	0.16 ± 0.04	6.10 ± 2.95	7.96	102.14	9
1698	Knight Nubble	0.24	47.80 ± 2.62	1.31 ± 0.76	10.44 ± 2.96	23.24 ± 2.65	5.30 ± 1.07	3.72 ± 0.83	2.86 ± 0.57	0.68 ± 0.52	3.00 ± 1.38	5.33 ± 1.92	6.16	103.69	5
	Light-Toned Sandstones	**0.12**	**48.19 ± 5.84**	**0.84 ± 0.14**	**10.79 ± 2.09**	**17.75 ± 3.11**	**8.34 ± 4.05**	**6.55 ± 8.02**	**2.10 ± 0.56**	**0.73 ± 0.24**	**0.32 ± 0.55**	**7.38 ± 6.90**	**3.93**	**102.99**	**61**
1683	AEGIS post 1683a	0.12	47.26 ± 5.67	0.87 ± 0.06	9.43 ± 1.99	15.08 ± 2.19	9.94 ± 5.42	7.31 ± 7.91	1.91 ± 0.53	0.70 ± 0.29	0.16 ± 0.03	8.67 ± 8.87	3.72	101.32	9
1684	AEGIS post 1684a	n.d.	46.32 ± 10.63	0.85 ± 0.25	11.71 ± 3.60	17.59 ± 4.17	6.29 ± 1.69	8.57 ± 10.03	2.28 ± 0.75	0.88 ± 0.37	0.14 ± 0.04	10.57 ± 12.29	0.85	105.20	9
1690	AEGIS post 1690a	0.1	51.61 ± 2.15	0.93 ± 0.04	11.67 ± 1.00	20.51 ± 1.30	6.60 ± 0.70	2.06 ± 0.56	2.44 ± 0.50	0.75 ± 0.16	0.26 ± 0.08	5.43 ± 1.73	3.79	102.24	9
1692	The Maypole	0.11	52.18 ± 1.53	0.93 ± 0.08	11.92 ± 1.61	18.30 ± 2.14	11.82 ± 2.75	1.96 ± 0.38	2.39 ± 0.19	0.62 ± 0.17	0.21 ± 0.08	2.88 ± 2.27	7.94	103.20	5
1695	Mount Gilboa	0.3	45.51 ± 3.28	0.67 ± 0.09	10.38 ± 1.14	15.55 ± 3.59	6.72 ± 5.07	15.13 ± 9.62	1.68 ± 0.49	0.70 ± 0.18	0.30 ± 0.21	5.17 ± 3.71	7.45	101.81	10
1700	Ripple Pond ccam	0.17	46.32 ± 4.25	0.85 ± 0.07	9.88 ± 1.56	18.56 ± 1.26	7.70 ± 2.49	5.92 ± 5.08	1.99 ± 0.43	0.68 ± 0.17	0.91 ± 1.15	10.05 ± 5.09	2.82	102.87	10
1705	Turtle Island	0.1	50.39 ± 2.53	0.86 ± 0.05	11.19 ± 0.90	19.07 ± 0.53	11.10 ± 3.39	1.98 ± 0.80	2.20 ± 0.23	0.72 ± 0.16	0.14 ± 0.02	6.87 ± 1.45	4.43	104.51	9

Note. The bold values represent the mean values for a large set of data, while the normal text is showing mean values for an individual target. [a]From Rivera-Hernandez et al. (2020). [b]$1\sigma = 1$ standard deviation of the variation of N points in the average LIBS observation major oxide compositions found in Table S1 in Supporting Information S1. [c]Predicted from the preliminary sulfate calibration method Clegg et al. (2020). [d]Hydrogen expressed as H_2O; From Thomas et al. (2020). [e]N = The number of LIBS observation points used to calculate the mean and standard deviation of the major oxide compositions. [f]n.d. = not determined.

have no or very little MnO within them, are not shown in Figure 1. Facies on the chemostratigraphic plot have been separated by type: Murray bedrock, other diagenetic features (e.g., dark mottling; Meslin et al., 2018), diagenetic concretions, dark-toned sandstones, and light-toned sandstones. Figure 1c shows the full traverse map with the Newport Ledge location labeled and Figure 1d shows a map with the locations, sol numbers, and 1 m contours in the area surrounding Newport Ledge. The Mn-rich targets are listed in Table 1.

There are notable differences in Mn occurrence within the different facies. Dark-toned concretions are observed embedded in bedrock, within calcium sulfate veins, and in dark-toned layers within bedrock, that are typically Fe, Mg, and P-rich, and occasionally Mn-rich, as shown on Figure 1b (Sun et al., 2019; L'Haridon et al., 2018; Meslin et al., 2018). Mn-rich observations in non-concretionary diagenetic features were found primarily in Sutton Island, and Mn-rich diagenetic concretions were found primarily in Blunts Point. The concretions found throughout the Murray formation are interpreted as likely due to multiple late-stage diagenetic events (L'Haridon et al., 2018; Meslin et al., 2018; Sun et al., 2019).

In addition, dark and light-toned sandstones with abundant MnO are also found at the Sutton Island to Blunts Point member transition (Figure 2) at a location called Newport Ledge. The Newport Ledge target was observed on Sol 1686 at −4,280 m elevation (at the sol 1685 location on Figure 1d); all observations of Mn-rich sandstones are confined to a ∼16 m elevation interval and to sols 1683–1705. The dark-toned sandstones have FeO_T enrichment up to 1.5× and less CaO and sometimes less MgO compared to the light-toned sandstones (Table 1). The enrichment of CaO and MgO in light-toned sandstones typically correspond to a sulfate component that is common in the Blunts Point bedrock (e.g., Nellessen et al., 2019; Sun et al., 2019; Thompson et al., 2020). Besides differences in FeO_T and MnO, the sandstones are not significantly different in composition from the typical Murray compositions of Sutton Island or Blunts Point. The chemistry, location, elevation, and sol number for each observation point described in Table 1 and the chemistry of the diagenetic targets and typical Murray points found in Figure 1b MnO chemostratigraphy are tabulated in Data Set S1 (Gasda et al., 2023).

The MnO abundance is quite variable between the observed dark-toned sandstones (Table 1). Most, but not all, of the dark-toned sandstones are enriched in manganese compared to the surrounding bedrock. Dark-toned sandstones have an average ∼10× enrichment of total MnO compared to the surrounding bedrock, have coarser grain sizes, and have high ChemCam oxide totals after including water as either H_2O, OH, or H and the preliminary SO_3 composition (Table 1) as determined by ChemCam (Clegg et al., 2020; Thomas et al., 2020). Table 1 and dataset show values that are not corrected for distance and are not renormalized to 100%. Most targets have >100% oxide totals on average, which can be due to uncertainty or distance effects. The oxide models are statistically valid up to ∼106% (Clegg et al., 2017), not including MnO, SO_3, or water. Longer distance measurements can cause a few percent inflation of SiO_2, Al_2O_3, Na_2O, and K_2O depending on the distance (Wiens et al., 2021). The mean Murray formation MnO value below VRR is 0.09 ± 0.05 wt% MnO (n = 3,551, 1σ) and the mean MnO concentration values for Sutton Island and Blunts Point members are similar. The dark-toned sandstone targets have a SO_3 content similar to the mean values of the Sutton Island and Blunts Point members. The light-toned sandstones have a more variable SO_3 content compared to dark sandstones (Table 1). Major element oxide weight totals near or above 100% indicate that these dark sandstones, unlike diagenetic features that are Mn-rich, do not contain a high abundance of a "missing component," that is, elements that ChemCam can detect but does not quantify, including phosphorous, carbon, and the halogens. In most of the dark-toned targets listed in Table 1, the spectra on the bedrock do not indicate the presence of P, C, or halogens (i.e., they are below the detection limit for ChemCam). The exception is the Denning Brook target, where weak P lines were observed in its spectra at three observation points. However, the oxide total for this target is high, and the P intensity is weak, so any P in this target is likely a minor component. The targets at this location are typically hydrated. The mean hydration of the bedrock in the dark-toned rocks is 6.94 wt.% H_2O, 2.5× greater than typical surrounding Murray bedrock (Thomas et al., 2020) and ∼1.8× greater than the light-toned sandstones (Table 1). Table 1 lists the estimated H_2O content for each target. Note that ChemCam cannot determine if the H present is H_2O, OH, or H within the rock, and thus the values listed in Table 1 are an upper limit. The H_2O content in Table 1 is not included in the oxide sum.

APXS data suggest similar results (Supplement Text S1). APXS reports less MnO but greater FeO_T content in the cross targets (Berger et al., 2020; Figure S8 in Supporting Information S1). MnO and FeO_T have negative correlations with SO_3 and no correlations with P_2O_5 (Figures S8–S9 in Supporting Information S1) or Cl (Figure S10 in Supporting Information S1). The SO_3, P_2O_5, and Cl content of these targets are similar to that of typical Murray

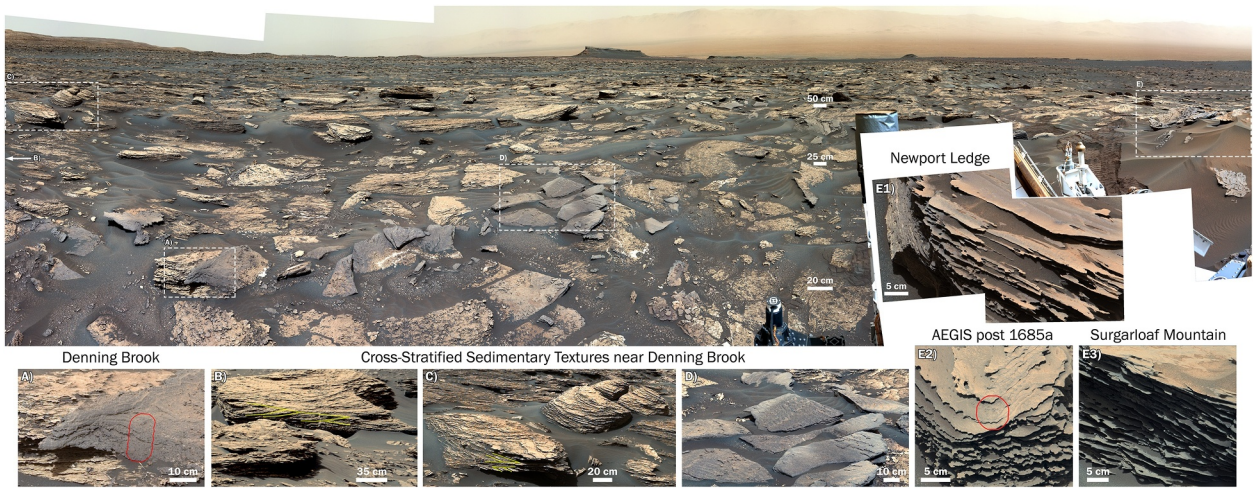

Figure 2. Mastcam mosaic from the sol 1686 rover location looking behind the rover (downslope) at the transition point between the Sutton Island and Blunts Point Murray members. Images from sols 1685–1689 display sedimentary textures of dark-toned Mn-rich sandstones and nearby rocks. Dashed line boxes in the large mosaic are shown as insets along the bottom of figure. Small red outlines show the approximate locations and extent of ChemCam observations (portions of the Remote Micro Imager images of these observations are shown in Figure 3). Throughout this transition area, dark-toned sandstones (presumably Mn-rich based on ChemCam observations at three locations) overlie light-toned materials. Insets from left to right: (a) Denning Brook, a Mn-rich fine-grained dark-toned sandstone ChemCam observation; (b) & (c) two light-toned blocks with cross-stratified textures, highlighted with yellow lines, 6 m away from Denning Brook and to the upper left in the large mosaic; (d) dark-toned materials (center of mosaic); and E1) Newport Ledge, E2) AEGIS post 1685a, E3) Sugarloaf Mountain, three thin planar laminated dark-toned sandstones. NASA/Caltech-JPL/MSSS.

targets with elevated MnO in all targets and elevated FeO_T in Newport Ledge (Berger et al., 2020; Figures S8–S10 in Supporting Information S1). The SO_3 versus CaO trend of these targets compared to that of typical Murray bedrock suggests that the variation of SO_3 is attributed to variations of Ca-sulfate cement in the bedrock (Berger et al., 2020; Figure S7 in Supporting Information S1).

Dark-toned Mn-rich sandstones are observed primarily at the Newport Ledge location (Figure 2). Although several targets were analyzed by ChemCam in this location, there are many additional blocks in the surrounding region that were not analyzed with ChemCam but appear in images to be similar in texture and albedo. At the transition zone between the Sutton Island and Blunts Point, dark-toned sandstones overlie light-toned materials stratigraphically. Denning Brook is a particularly Mn-rich fine-grained dark-toned sandstone target with up to ~4 wt% MnO (Figure 2a). Dark-toned materials are also found just to the right of Denning Brook (center of large mosaic in Figures 2a and 2d, Figure S9 in Supporting Information S1). Other blocks appear more laminated, such as ChemCam targets Newport Ledge (Figure 2e1, up to ~3.1 wt% MnO), AEGIS post 1685a (Figure 2e2, up to ~3.7 wt% MnO) and image-only target Sugarloaf Mountain (Figure 2e3) are all thin planar laminated dark-toned sandstones. Three more dark-toned sandstones were observed by ChemCam up to 5 m above Newport Ledge: Mason Point, Mitchell Hill, and Knight Nubble (the dark-toned sandstone target with the highest MnO, up to ~4.5 wt% MnO) were all dark-toned fine-grained sandstones.

In addition to the dark-toned Mn-rich sandstones, there were observations of light-toned sandstones that sometimes contain high abundances of Mn. Ripple Pond is light-toned and very fine to fine-grained sandstone with up to ~3.5 wt% MnO. Two similar light-toned blocks with cross-stratified textures (Figures 2b and 2c) are located 6 m away from Denning Brook.

Although the sandstone targets described above show elevated MnO abundances that are typically at least twice as enriched as the surrounding bedrock, not all sandstones in this area are Mn-rich. For example, Mitchell Hill and Mason Point are dark-toned sandstones with mean compositions of 0.16 wt.% MnO (Table 1). Generally, the light-toned sandstones have lower MnO than dark-toned sandstones.

Much of the bedrock at these locations shows extensive evidence of groundwater activity before and after lithification. The primarily mudstone members in the Murray tend to host calcium sulfate veins (Figure S7 in Supporting Information S1) along with occasional observations of other water-soluble salts including Mg, S, Cl, and B (Das et al., 2020; Gasda et al., 2017; Lanza et al., 2014; Nachon et al., 2014, 2017; Rapin et al., 2016, 2019;

Schwenzer et al., 2016; Thomas et al., 2019). Bedrock bordering filled fractures is sometimes altered to form high silica materials (Frydenvang et al., 2017; Yen et al., 2017). At least two episodes of calcium sulfate vein formation may have occurred in the light-toned material in Blunts Point, as evidenced by both sub-horizontal and cross-cutting vein occurrences, and the sub-horizontal veins may have formed during an early diagenetic event (e.g., Siebach et al., 2014; Figures S11–S14 in Supporting Information S1). Calcium sulfate cement is also likely present in Blunts Point materials (Nellessen et al., 2019; Sun et al., 2019; Thompson et al., 2020). For example, the underlying strata shown in Figure 2 display light-toned sub-horizontal layers that are consistent with veins observed in other Blunts Point bedrock (Figures S12 and S13 in Supporting Information S1). In addition, while the AEGIS post 1686a target (not shown in Figure 2) is Mn-rich, with up to ∼1.0 wt% MnO, 5 out of 9 observation points that appear to hit bedrock just above a sulfate rich layer (Figure S28 in Supporting Information S1) have high CaO (up to ∼19 wt%) and SO_3 (up to ∼21 wt%), and two of the points have elevated Na (up to ∼11 wt%) and Cl. Hence, we excluded this target from our analyses because of the particularly high amount of sulfate and Cl in this target compared to others in this location, which makes it difficult to determine the target bedrock composition.

In addition to assessing sedimentary textures, grain size was also reported by Rivera-Hernández et al. (2020) for all study targets using the GINI Index and with image-based grain size analysis (Figure 3). A higher GINI index value for ChemCam targets suggests coarser-grained materials, assuming a relatively homogeneous chemical composition within the bedrock. Analysis of grain size in MAHLI and ChemCam RMI images indicates that both dark-toned and light-toned surfaces shown in Figure 3 are sandstones. In general, the dark-toned sandstones have higher GINI indices (i.e., coarser grained) compared to light-toned sandstones (Table 1). Both types of sandstones are coarser grained than the surrounding typical Sutton Island and Blunts Point Murray. The Newport Ledge target (Figure 3a, MAHLI, and Figure 3d, ChemCam RMI) displays 0.1 mm dark- and light-toned grains within a fine-grained matrix, indicating that Newport Ledge is a very fine to fine sandstone on the Wentworth Scale (Wentworth, 1922). ChemCam RMI images of AEGIS post 1685a and Denning Brook (Figures 3c and 3e, respectively) show grain sizes up to 0.25 mm, which is a coarse silt to fine-grained sandstone on the Wentworth Scale (Wentworth, 1922). Denning Brook has a low GINI Index value (fine silt) compared to the AEGIS post 1685a target, which has a higher GINI Index value (medium sand). Each of these sandstone targets is compared to the MAHLI image of Cassongue (Figure 3b), a typical Sutton Island outcrop from lower in the section (sol: 1482; elevation: −4,367 m). Cassongue is a light-toned and very fine-grained rock with common calcium sulfate veins. Grains are not discernible in the MAHLI image of Cassongue; therefore, the rock is likely to be very fine silt or mudstone.

In summary, the Mn-rich dark-toned sandstones are confined to a 16 m elevation interval and primarily observed near Newport Ledge, which represents the transition from Sutton Island to Blunts Point. The Sutton Island member is composed of heterolithic mudstone and sandstone, while the Blunts Point member is a return to finely laminated mudstone. The Mn-rich dark-toned sandstones have the highest GINI Index (inferred coarse grain size) and higher mean MnO and hydration compared to surrounding light-toned sandstone and Murray bedrock mudstone. The Mn-rich dark sandstones tend to be similar to typical Murray compositions with elevated MnO, FeO_T, and hydration.

4. Discussion

In the following section, we discuss the sedimentary interpretation of the planar dark-toned sandstones and nearby cross-stratified sediments at the Newport Ledge transition, and then discuss different mechanisms that could have led to enrichment of MnO in these sandstones, including diagenetic and authigenic precipitation. In addition, we discuss the possible oxidants responsible for Mn oxide precipitation and the astrobiological implications of these deposits.

4.1. Deposition of Sandstone at Newport Ledge in a Subaqueous Plume Environment

As previously discussed, Gale once hosted a crater lake or series of lakes during its long lacustrine history (e.g., Grotzinger et al., 2015). Within these lakebed sediments, the rover encountered a transition from a heterolithic mudstone and sandstone member to a primarily laminated mudstone member at the Newport Ledge location (Edgar et al., 2020). This is interpreted by Edgar et al. (2020) as a transition from a marginal lake or lake depositional setting (shallow water levels) to a suspension fall-out lacustrine (deeper, stable water levels)

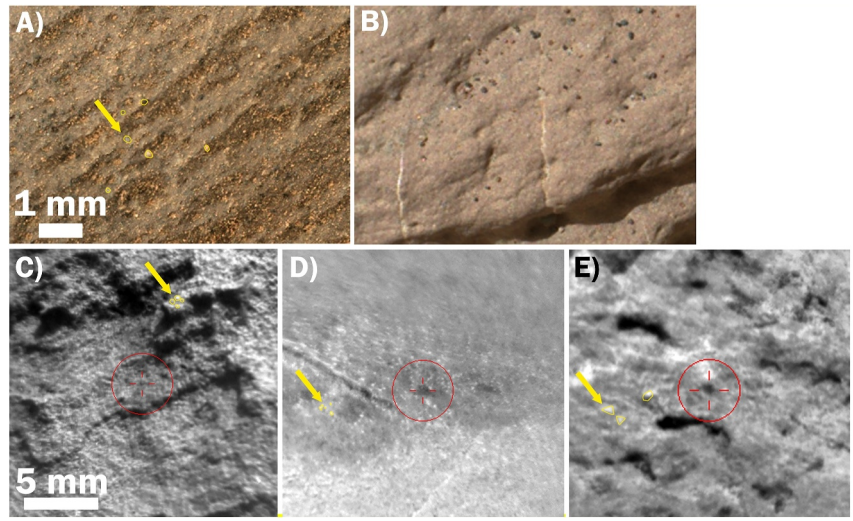

Figure 3. (a, c–e) Images of dark-toned sandstones classified by the GINI Index (Rivera-Hernández et al., 2019) as coarser grained. Yellow arrows point to individual grains. Some grains in images are outlined with yellow dotted lines. Mars Hand Lens Imager (MAHLI) images (a)–(b) are shown at the same 1 mm scale. Remote Micro Imager (RMI) images (c)–(e) are shown with the same 5 mm scale. (a) MAHLI image (cropped from full 15 mm standoff image) of Newport Ledge display ~0.1 mm dark and light toned grains (very fine to fine sand) within a fine-grained matrix. Compare to (b) MAHLI of Cassongue target, a typical Sutton Island Murray target from lower in the section (sol: 1482; elev: −4,367 m), a light-toned very fine grained material with surficial regolith grains for comparison, and with common calcium sulfate veins. Grains are not discernible in the MAHLI image of Cassongue; therefore, the rock is likely to be very fine silt or mudstone. RMI images of AEGIS Post 1685a (c), Newport Ledge (d), and Denning Brook (e) show grain sizes of up to 0.25 mm (coarse silt to fine grained sandstone). Image credit: NASA/Caltech-JPL/MSSS.

depositional setting. Sutton Island could represent a setting where fluvial channels transported water and sediments into a nearby lake, potentially via isolated pools connected by river channels, facilitating spatially and stratigraphically variable deposition of sand and mudstone (e.g., Gwizd et al., 2022, 2023; Rapin et al., 2019). Evaporation of these lakes and pools causes the formation of desiccation cracks (Stein et al., 2018). Blunts Point may have formed in a primarily deeper sub-aqueous depositional environment where thin mm-to cm-sized mudstone laminae were deposited (Edgar et al., 2020; Rapin et al., 2019; Rivera-Hernández et al., 2020). Planar sandstones have also been observed in Hartmann's Valley member of Gale crater, and these were interpreted as interdune aeolian bedforms (Gwizd et al., 2022). However, this interpretation was based on the larger scale of the outcrops and the intervals of cross stratified sandstones in those outcrops that likely indicate a dune setting (Gwizd et al., 2022). Blocks in Sutton Island are more broken up than in continuous outcrops, making this interpretation more difficult; Gwizd et al. (2023) showed that the changes in Sutton Island bedrock likely represent a change in lake water level. The higher portion of Sutton Island likely represents the channel outlet near the shore of the lake (Gwizd et al., 2023). Additionally, Colombera and Mountney (2019) have shown that planar and cross-stratified sandstones tend to be more prevalent in the channel deposits of braided river deposits, and planar horizontally bedded sands are more prevalent in ephemeral river channel deposits. This is consistent with the likely braided river and lake margin environment of Sutton Island (Edgar et al., 2020; Fedo et al., 2017, 2018; Gwizd et al., 2018, 2019, 2023). Planar laminated sandstones may also be deposited just offshore in the flow channels of delta (Zavala & Pan, 2018) sometimes during flood events (e.g., Lang et al., 2004). Thus, it is likely that these sandstones were deposited in a channel deposit either in a river or a delta, and the delta interpretation is more consistent with the current hypothesis of this location (e.g., Edgar et al., 2020; Fedo et al., 2017, 2018; Gwizd et al., 2023).

The depositional interpretation has important implications for the types of materials that are expected to be deposited in different parts of the lake system. In a fluvial deltaic system, sand is commonly deposited in channels and at the mouth of the delta as it enters a lake. Plumes of material transported by the water enter the lake; the material deposited by the flow tends to become finer with distance away from the shore and away from the plume axis where the transporting water slows. The sedimentary structure of the deposit is also strongly controlled by the distance from the channel axis, with planar laminated sandstones and ripple textures found at the margins of the

flow channel (Zavala & Pan, 2018). Thus, if the observed sandstones in Gale formed in an aqueous environment, it is likely they formed at the margins of channels or within lobes exiting a subaqueous delta. This hypothesis is strengthened by the observation of other traction and fall-out textures, with fall-out textures (e.g., finely laminated mudstones) beginning to dominate at locations further along the traverse, which would have been offshore and up section from Newport Ledge (Figure 2), and after deposition of Newport Ledge.

Several observations (Figure 2) of materials near Newport Ledge indicate they could be associated with a plume or lake margin depositional setting. Figures 2b–2d shows three examples of cross-stratified sedimentary textures, including dark-toned possible ripple textured materials and light-toned materials, some of which are cross-stratified. Such cross-stratification is consistent with possible traction transport in fluvial deposits and could be an indication that these materials were deposited in a flow channel either at the mouth of a delta or just off-shore in very shallow water. Figure 2e1–2e3 shows that just a few meters away, Newport Ledge, AEGIS post 1685a, and Sugarloaf Mountain are all planar laminated sandstones. Planar sandstones are more likely to be deposits along the margin of a subaqueous plume or flow channel.

A generalized model of the near-shore region of the lake (based on Edgar et al., 2020; Gwizd et al., 2022, 2023; Rapin et al., 2019; Rivera-Hernández et al., 2020), is shown in Figure 4. In this model, there was an updip fluvial system that upon entering the lake generated a delta with sediment plumes extending into the lake and depositing material in a subaqueous environment. This type of near-shore depositional environment typically has a high degree of spatial variability. Coarse-grained materials tend to be deposited within channels and close to shore (Zavala & Pan, 2018). Thus, fine sandstones and coarse silt are most likely deposited along the margins of active and previously active channels near the base of the subaqueous upper fan to mid-fan areas (orange and light brown in Figure 4). Planar sandstones similar to Newport Ledge (Figures 2e1–2e3) would likely to be deposited in the part of the system shown in pink.

4.2. Evidence of Diagenetic Precipitation and Alteration of Mn Deposits

Before assessing a potential authigenic origin, we assess whether a diagenetic process can explain the observed chemical and morphological features of the Mn in these sandstone materials. Multiple lines of evidence suggest that these sediments were patchily altered by groundwater over multiple events, consistent with observations elsewhere in the crater (e.g., Gasda et al., 2022). These observations include the presence of Mn-enrichments that are sometimes associated with P high enough to be detected by ChemCam (Gasda et al., 2022; Treiman et al., 2023) or are strongly correlated with MnO and P (Berger et al., 2020). However, the dark-toned sediments at Newport Ledge do not typically contain P detectable by ChemCam. APXS data show that P_2O_5 and MnO or FeO_T have a no clear correlation in these targets. Targets elsewhere in the Murray can have both high MnO and P_2O_5, and have been identified as nodules (Berger et al., 2020). P_2O_5 composition is similar to that of the typical Murray bedrock (Berger et al., 2020; Supplementary Text S1). Thus, P in these targets likely reflects typical bedrock variation rather than addition due to the diagenesis that resulted in Mn-enrichment. Second, sulfate within the matrix that likely formed prior to lithification occurs in materials throughout Murray and at this location, in addition to the cross-cutting veins that would only occur post-lithification. Hence, it is difficult to fully constrain the formation of the manganese enrichment in the dark-toned sandstones; manganese enrichment at Newport Ledge may have formed by a separate event from the others observed here (details below), potentially before lithification due to the higher permeability of sandstones compared to mudstones. Cross-cutting sulfate veins would have only formed post-lithification in these targets.

Silt and sand are coarser grained and have higher permeability as compared to the surrounding mudstone deposits. While the Mn-rich sandstones lack enrichment or positive correlations with water soluble anion groups such as sulfates, phosphates, chlorides, or carbonates, Mn can be precipitated from a fluid as the result of oxidation. The lack of enrichment or positive correlations with other soluble species indicates that the alteration fluid did not contain elevated amounts of these elements or did not experience conditions that would cause those materials to precipitate. Given the affinity of P adsorption to Mn oxides (Yao & Millero, 1996), the lack of P enrichment in the dark sandstones indicates that the fluid was likely not enriched in P.

The calcium sulfate veins that crosscut bedding commonly occur in light-toned materials and less commonly in dark-toned planar laminated sandstones (e.g., Newport Ledge). Light-toned sandstones have a greater variability in sulfate content, possibly due to variations in permeability pre-lithification, compared to the dark-toned planar laminated sandstones. Dark-toned sandstones tend to have a sulfate abundance near the mean value for Sutton

Island, and thin to hairline veins observable in ChemCam RMIs (Figure S10 in Supporting Information S1). The presence of the veins suggests that the sandstones experienced Ca sulfate vein formation post-lithification, which is common in the Murray formation (Supplement Text S2). ChemCam data also suggest that Ca and Mg sulfate is likely present within the matrix of the sandstone targets, which is a common observation within the Murray formation (Figure S12 in Supporting Information S1; Edgar et al., 2020; Rapin et al., 2019; Rivera-Hernández et al., 2020). The presence of the sulfate suggests that Mg and Ca sulfate-rich groundwater permeated through all of the strata pre-lithification to a variable extent, consistent with interpretations by Berger et al. (2020). Sub-horizontal veins are also observed in Blunts Point (e.g., Nellessen et al., 2019; Sun et al., 2019; Thompson et al., 2020) that are cross-cut by the later stage calcium sulfate filled fractures (e.g., Figure S12 in Supporting Information S1). The dark-toned sandstones lack sub-horizontal veins, and thus dark-toned sandstones and Blunts Point materials are different.

Although the Mn-rich concretions near Newport Ledge could have shared a common source with the Mn found in the dark-toned sandstones, it is more likely that these features formed during separate events based on their different chemistry and morphologies. The diagenetic features and concretions observed throughout nearby strata are occasionally Mn-rich (Figure 1b; L'Haridon et al., 2018; Sun et al., 2019), but they are not morphologically similar to dark-toned veins observed previously by Lanza et al. (2016) or later by Gasda et al. (2022). These concretions may be similar to those observed by Treiman et al. (2023) later in the mission. The chemistry of the diagenetic features tends to have a greater abundance of trace elements, including P (e.g., Lasue et al., 2016; L'Haridon et al., 2018; Meslin et al., 2018; Sun et al., 2019; Treiman et al., 2023), and importantly are not always Mn-rich. In addition, the morphological differences between the diagenetic features described by Sun et al. (2019) and the dark-toned sandstones may indicate that the diagenetic features and concretions formed through multiple generations of groundwater diagenesis to account for variations in their chemistries (L'Haridon et al., 2018; Meslin et al., 2018; Sun et al., 2019). The lack of potential anion enrichment in the dark-toned sandstones is further evidence that manganese is likely present as an oxide mineral and that the dark sandstone Mn deposit formed in a different fluid alteration event.

Enrichment of typically minor elements (e.g., P, Cl) within diagenetic features and concretions could indicate a different mineralogical host for the Mn (e.g., phosphate). On Earth, Mn oxides precipitated within organic-bearing sediments are dissolved after microbial reduction, which can lead to Mn-carbonate precipitation due to liberated bicarbonate and Mn^{2+} over short timescales (Kristensen et al., 2003). The ChemCam data for the dark-toned sandstones in Gale crater are not consistent with carbonate formation. If carbonate is not available or if phosphate is very abundant, Mn-phosphates will form readily (Johnson, Savalia, et al., 2016). Amorphous Fe, Al, and Mn oxides also efficiently scavenge phosphate by adsorption and co-precipitation, especially in oxidizing and alkaline conditions (e.g., Johnson, Webb, et al., 2016; Moore & Reddy, 1994; Yao & Millero, 1996). Scavenging of P or Mn/Fe-phosphate formation from a P-rich fluid may provide a mechanism for the Mn and P-rich diagenetic features, such as the dark-toned concretions which are embedded in Ca sulfate fracture fills (L'Haridon et al., 2018; Meslin et al., 2018; Sun et al., 2019; Treiman et al., 2023).

Hence, the Mn precipitation in sandstones, the Mn precipitation in P-rich diagenetic features, the Mg and Ca sulfate cementation, and the vein formation were all likely formed by separate groundwater fluid events. The Mn oxide and Ca and Mg sulfate precipitation events both occurred before the vein formation event, but it is difficult to determine the relative timing of the sulfate and Mn oxide precipitation events. They both likely formed during the early diagenetic stage of alteration pre-lithification. The proximity of all these types of materials and varied chemistries is a further indication that the Gale crater experienced multiple diagenetic and groundwater events over long timescales. Changes in permeability and porosity of the bedrock can manifest in the spatial/stratal differences observed by the rover (Comellas et al., 2022; Gasda et al., 2022) and are consistent with other interpretations of diagenesis in Gale (e.g., Achilles et al., 2020). Early diagenetic fluids that formed phyllosilicates in Gale crater were likely alkaline (pH ~8–9) and contained too little CO_2 to form significant carbonate deposits (Turner et al., 2021), which would have favored Mn^{2+} remaining in solution if the fluids were sufficiently reducing (e.g., Figure S11 in Supporting Information S1). A change in redox or pH—for example, coupling with an oxidant-rich atmosphere or oxidized lake water—would be required to precipitate the Mn^{2+} from the groundwater solution (e.g., Gasda et al., 2022; Lanza et al., 2022).

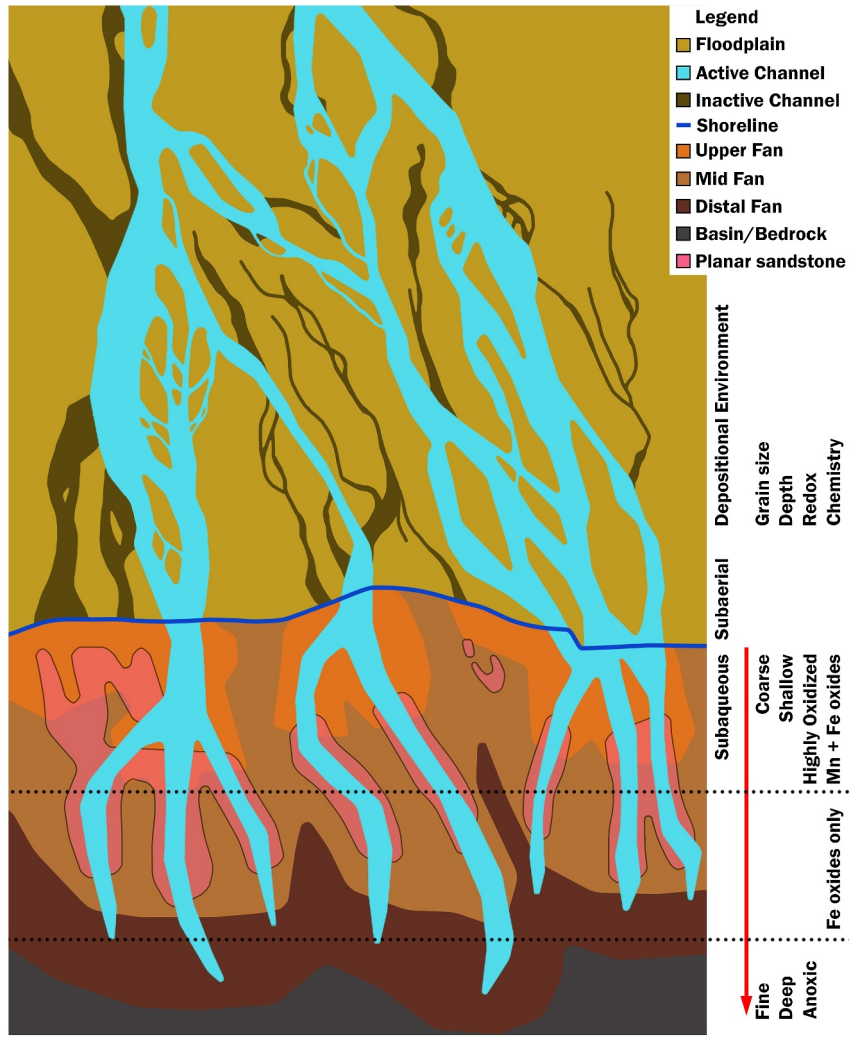

Figure 4. Illustration of the Sutton Island/Blunts Point transition area based on the Gwizd et al. (2023) and Fedo et al. (2018) model: a braided channel and offshore subaqueous delta formed by plumes of discharged material. Pink areas are locations where dark-toned planar sandstones may be deposited in the delta deposit in relation to distance from shore and distance from the channel axis. Labels in the bottom right show how grain size, depth, redox, and chemistry are expected to change as one moves offshore, assuming an oxidant-rich atmosphere.

4.3. Manganese Precipitation in Near-Shore Sandstones

The possibility that these Mn deposits at Newport Ledge are authigenic Mn oxides is difficult to explain with the current state of knowledge of possible oxidation processes on Earth without biological activity, oxygen, or both. While Fe^{2+} reacts spontaneously and rapidly with oxygen under circumneutral pH to form Fe^{3+} oxides, the oxidation of Mn^{2+} with oxygen only proceeds at appreciable rates (100 years or less) below pH 9 with microbial catalysis (Kessick & Morgan, 1975; Tebo et al., 2004; Yu & Leadbetter, 2020). The abiotic half-life of oxidation (i.e., the reaction rate) for Mn oxidation is 10^4–10^5 years for modern Mars atmospheric levels of oxygen (Figure S16 in Supporting Information S1). Globally, Mars valley networks took up to 10^7 years to form (Hoke et al., 2011) and Gale crater would have been active during this period of Mars (Vasavada, 2022). Any instance of lake level would only last a fraction of the total time the lake was active. Thus, the precipitation of Mn oxide would need to occur on short timescales. An estimate where it takes $\sim 10^6$ years to form ~4 km of lake sediments in the crater would suggest that in 1,000 years, the sediment level increases by 4 m if sedimentation occurs at a constant rate. A rate of 4 m per 1,000 years is enough to bury the sandstones and prevent the process of atmospherically coupled oxidation of Mn from occurring. Since the rate of Mn oxidation needs to outpace the average estimated sedimentation rate, much more oxidant is required in the Mars atmosphere (see later discussion). On the

other hand, microbially mediated oxidation occurs in days to weeks (Yu & Leadbetter, 2020). This microbial catalysis can be enzyme-mediated (van Waasbergen et al., 1996) or can occur due to chemical reactions with reactive oxygen species (e.g., superoxide or hydrogen peroxide) that are produced from bacterial and fungal enzymes interacting with oxygen (Hansel et al., 2012; Learman et al., 2011). Emerging evidence suggests that anoxic oxidation may occur through a bacterial photosynthetic pathway (Daye et al., 2019; Johnson et al., 2013). This possible anoxic but biological pathway for Mn oxide formation requires light, and would therefore be confined to shallow waters. Abiotic, photochemical oxidation of Mn^{2+} is not thought to be a viable pathway when Fe^{2+} is present or at wavelengths >240 nm (Anbar & Holland, 1992). Photochemically produced reactive oxygen species in nitrate- and oxygen-bearing solutions can oxidize Mn^{2+}, but this has only been demonstrated at pH 8.9 and above (Jung et al., 2017).

Previous work suggests that Gale lake was likely redox stratified with respect to iron, based on the hematite-bearing facies of the Murray formation being encountered at higher elevations, and magnetite-bearing facies at lower elevations in Pahrump Hills (Hurowitz et al., 2017) and later on VRR (David et al., 2020; L'Haridon et al., 2020). The dark- and light-toned sandstones investigated here likely formed in a shallow sub-aqueous deltaic setting (Figure 4). On Earth, shallow near-shore waters are typically strongly oxidizing environments due to interaction with the atmosphere (e.g., Frakes & Bolton, 1984). Dissolved Mn^{2+} and Fe^{2+} will precipitate as Fe^{3+} and Mn^{4+} oxides in these environments (Figure S15 in Supporting Information S1). The lack of significant "missing components" in Table 1 or trends between Mn and other elements (e.g., Berger et al., 2020, 2022; Frydenvang et al., 2020) indicates that Mn enrichment in the dark and light-toned sandstones are likely to be Mn oxides, rather than reduced manganese in carbonate, sulfide, phosphate, or halide minerals, which are more likely to form diagenetically (Johnson, Webb, et al., 2016) as discussed above. The slight (~1.5×) FeO_T enrichment in these bedrock targets suggest that Fe and Mn precipitation are decoupled in this system; that is, the groundwater is high in Mn but not particularly enriched in Fe.

There are several possibilities for a precipitation model of authigenic Mn oxides at Newport Ledge based on aquatic settings on Earth. Considering evidence for redox-stratification of Fe within the mineralogical facies of the Murray Formation (Hurowitz et al., 2017), oxidation of lakewater Mn^{2+} would be expected to occur at the oxic-anoxic interface, where enhanced surface oxygen concentrations encounter elevated Mn^{2+} concentrations, such as in modern terrestrial redox-stratified marine basins and lakes (Jones et al., 2011; Lewis & Landing, 1991; Tebo et al., 1984). However, due to the reductive dissolution of Mn-oxides under anoxic conditions (Calvert & Pedersen, 1996; Jones et al., 2011), precipitation of Mn oxides from redox-stratified basins and lakes generally occurs only at depths corresponding to the anoxic-oxic boundary, producing a "bathtub ring" of Mn-oxides and/or diagenetic Mn-carbonates (formed after reduction of Mn oxides within sediments) at this depth (Force & Maynard, 1991). A similar scenario is implied for Gale by the Hurowitz et al. (2017) redox-stratified lake model. The bathtub ring precipitation should depend on depth-dependent chemistry, not sediment texture. While the Newport Ledge Mn oxides occur at a discrete elevation interval (Figure 1b), and Mn is preferentially associated with sandstones (Table 1), we also observe a slight increase in the MnO in the bedrock that is ~2× greater than lower Sutton Island bedrock that peaks at the Sutton Island to Blunts Point transition (Figure 1b). This increase in MnO in the bedrock could be indicative of a bathtub ring of Mn. However, the rover only crossed this chemo-stratigraphic transition in one location, so we do not have clear evidence of a laterally extensive bathtub ring. Another inconsistency with the bathtub ring model for Newport Ledge is that the anoxic-oxic boundary in many terrestrial basins and large lakes is often quite deep, 100–200 m or more (Force & Maynard, 1991), as it is stabilized by density and thermal gradients. The shallow deposits at Newport Ledge seem incompatible with formation at a deep anoxic-oxic interface.

An alternative scenario for Mn-oxide precipitation in a redox-stratified basin is the periodic input of cold, dense oxygenated water that allows the entire water column to become oxygenated. Such events produce sedimentary horizons of authigenic Mn oxides, such as in the Baltic Sea (Huckriede & Meischner, 1996). Although a river system is implicated by the delta model (Figure 4; Edgar et al., 2020; Gwizd et al., 2023; Rapin et al., 2019; Rivera-Hernández et al., 2020), and could be a source of freshwater, it is difficult to envision a selective mechanism by which only some sandstones would be sites of preferential Mn oxide precipitation related to periodic oxidation.

Ferromanganese deposits are widespread in the shallow, oxic portion of terrestrial lakes, including the Laurentian Great Lakes, in the northern hemisphere, and occur as grain coatings, crusts, nodules, and concretions (Callender

& Bowser, 1976). Ferromanganese crusts form through reductive dissolution of Fe and Mn oxides under anoxic conditions occurring at shallow depths within organic-rich sediment porewaters, such that Fe^{2+} and Mn^{2+} are produced, and can diffuse toward the oxic-anoxic interface at the top of the sediment where they re-precipitate as a crust (Froelich et al., 1979; Gorham & Swaine, 1965). The FeO_T enrichment is only minor in the Gale dark-toned sandstones, but mechanistically, these terrestrial lakes could be analogous to what is observed in Gale. Due to the requirement for a reductant, usually organic carbon, this process tends to occur in fine-grained near-shore sediments. Given the preferential association of Mn in sandstones rather than mudstones at Newport Ledge, and the lack of evidence for abundant organic material, this reduction-re-oxidation process also seems unlikely.

Most similar to the dark- and light-toned sandstones of this study are the freshwater ferromanganese grain coatings mentioned above. Grain coatings are commonly found on coarse-grained sands and gravels swept free of finer material in relatively high-energy water but not on finer-grained material (Cronan & Thomas, 1970). The source of Mn for freshwater ferromanganese deposits has not been extensively investigated but might include river water, anoxic sediment porewaters, or anoxic groundwater (Callender & Bowser, 1976). At one site, Trout Lake, Wisconsin, U.S.A., ferromanganese deposits were associated with syndepositional anoxic groundwater discharge through the sediments themselves, due to higher hydraulic conductivity associated with coarser-grained sand and gravel lenses (Krabbenhoft & Anderson, 1986). Upon discharge of anoxic groundwater into the oxic lakewater, Mn oxidation and precipitation occur at the sediment-water interface.

Given all the possibilities for ferromanganese precipitation discussed above, the most likely scenario for Mn precipitation of the Newport Ledge is preferential discharge of groundwater through more permeable sands into the more oxidized shallow waters of a redox-stratified Gale lake. Anoxic groundwater likely transported dissolved Fe^{2+} and Mn^{2+}, forming a redox front where Fe is precipitated deeper within the sediment than Mn, corresponding to a redox front beginning at the sediment-water interface and extending deeper into the sediment (e.g., Charette et al., 2005; Dean et al., 2006). Newport Ledge shows evidence for groundwater input prelithification in the presence of intermittent Ca and Mg sulfate deposits, which are disseminated in mudstones and sandstones in the same stratigraphic interval and are interpreted as early diagenetic salts (Rapin et al., 2019). Thus, a plausible mechanism for the formation of Mn oxides on sandstones is through preferential discharge of anoxic groundwater through these more porous sands with small spatial variations due to small differences in porosity and permeability of the bedrock.

The model for deposition of planar sands at Newport Ledge with the general increase of MnO within bedrock at this stratigraphic level suggests that the lake waters were shallow at the time of deposition, whether because the region was near the shore or because subaqueous sediments otherwise built up to produce a shallow zone (Figure 4). A sufficiently shallow deposit (e.g., over a low elevation gradient or in the top layers of the fan deposit) would allow the formation of Mn- and Fe-rich planar sandstones in the upper to mid subaqueous fan deposit (Figure 4), while deeper sandstone deposits would most likely lack elevated Mn. If the deepest part of the fan was below the oxic-anoxic interface, it could preclude the precipitation of Fe oxides. If Mn-oxides were brought into a deeper part of the fan by the plume at the mouth of a delta, any Mn oxide present would be unstable and would be dissolved (Figure S11 in Supporting Information S1). This, along with the general patchiness of alteration seen throughout the crater (Gasda et al., 2022), is consistent with the observation that not all sandstones in this region are rich in Mn. Ferromanganese nodule formation in the near-shore environment is common in lakes (Rossmann & Callender, 1968, 1969; Mothersill & Shegelski, 1973). The observation of nodules (e.g., Meslin et al., 2018; Sun et al., 2019), some of which are Mn-rich near this location, is consistent with the lake shoreline hypothesis.

4.4. Implications of Mn-Bearing Sandstone Deposits in Gale Crater

High Mn enrichment of sediments in Gale crater or Mars was not initially expected, but recent evidence has shown that Mn veins, nodules, and cement occur throughout the crater in certain locales and point to various fluid pH and redox conditions and multiple diagenetic events (Frydenvang et al., 2020; Gasda et al., 2022; Lanza et al., 2016, 2022; L'Haridon et al., 2018; Meslin et al., 2018; Treiman et al., 2023). Gale crater may have a post-impact hydrothermal component to its alteration history (e.g., Schwenzer et al., 2012) that would have facilitated greater Mn extraction from the surrounding crust (Gasda et al., 2022). Manganese would have remained in the groundwater in Gale if this groundwater remained reducing, if little dissolved CO_2 was present, and pH remained <10 as observations at this location in Gale thus far preclude the presence of carbonates. Recent thermochemical modeling suggests that sediments in the crater below VRR were altered with a pH range of 7.9–9.3 (Turner

et al., 2021), which is well within the range needed to preserve Mn^{2+} in groundwater fluids with low CO_2 and reduced with respect to Mn oxide formation (Figure S15 in Supporting Information S1). If this groundwater interacted with an oxidant near a redox boundary, precipitation could occur. On Earth, the oxidant is oxygen in the atmosphere, catalyzed by microbial activity (see earlier discussion). So far, there is no clear evidence of past life on Mars; thus, we need to explore options of what oxidants may have been present to account for the Mn enrichment found in the sediments in Gale.

Regardless of the emplacement model, the presence of elevated Mn within the sandstone suggests the interface of reducing fluid to transport Mn^{2+} with an oxidized fluid to oxidize and precipitate Mn. Manganese precipitation requires water, strongly oxidizing conditions (and/or biological activity, on Earth), and time. Mn oxide precipitation on Earth occurs readily near shallow shores of lakes and in groundwater due to the Earth's oxygen-rich atmosphere, but even under terrestrial conditions the reaction is kinetically very slow without microbial catalysis (Figure S16 in Supporting Information S1; after Johnson et al., 2013). On the other hand, both Mn and Fe are quickly reduced in anoxic environments within days and the Mn reprecipitates as Mn carbonate, if organic carbon is available (Kristensen et al., 2003) or as a phosphate either in P-rich brines or due to amorphous Fe and Mn oxide scavenging P (Johnson, Savalia, et al., 2016, Johnson, Webb, et al., 2016; Moore & Reddy, 1994; Yao & Millero, 1996). Although there is no evidence for elevated C in these targets and any C component is unlikely due to the high oxide totals, C is difficult to measure with ChemCam (Beck et al., 2017); thus, Mn carbonates are difficult to completely rule out. Siderite has been detected in higher stratigraphic levels in Gale crater, and minor Mn in those phases could be a possible pathway from which to form later Mn-rich fluids (Gasda et al., 2022; Thorpe et al., 2022). Significant enrichment of P are only found by ChemCam in targets likely altered by groundwater during late-stage diagenetic events. At modern Earth levels of oxygen, the half-life of the aqueous oxidation reaction is 10–1,000 days depending on whether the Mn oxidation is surface catalyzed or not, whereas under modern Mars conditions, the half-life is 10^4–10^5 years, assuming sufficient water could persist for long enough on the martian surface (Figure S16 in Supporting Information S1). The reaction proceeds much slower under drier conditions. If Mars had sufficient oxygen in its atmosphere, at least 1% of the oxygen in Earth's present atmosphere, then precipitation of Mn oxides could have progressed on a 10–100 years timescale, and this is likely sufficiently short to precipitate the oxides in a constantly changing braided river delta environment and to outpace the average sedimentation rate.

Oxygen is the strongest candidate for the Mn oxidizing agent because it is the most potent oxidizer that could form naturally at high enough abundance to oxidize all the Mn observed in the crater. Many terrestrial examples of Mn deposits coincided with the GOE. Pre-GOE, insufficient numbers of oxidants were present on Earth to produce widespread Mn deposits. The amount of oxidants produced by UV photolysis is insufficient to produce significant quantities of Mn oxides in Fe-rich deposits that formed pre-GOE (Anbar & Holland, 1992), which is supported by the relative lack of Mn deposits of pre-GOE age. A widespread oxidizing environment may not be required to produce Mn deposits if microbes are involved. Ostrander et al. (2019) recently showed that MnO deposits could have formed near nascent O_2 producing photosynthetic life prior to the GOE (~2.5 Ga). Johnson et al. (2013) hypothesized that anoxygenic photoautotrophic organisms could have produced substantial Mn oxide deposits in an O_2-poor environment at ~2.4 Ga. However, microbial-driven Mn-oxidation is unlikely on Mars given the lack of definitive evidence for life. Questions also remain as to how O_2 can form on Mars abiotically (Noda et al., 2019) and other candidate oxidants are not adequate to oxidize Mn in water. Perchlorate, which was likely dissolved in Gale surface and subsurface water (e.g., Clark et al., 2021), is kinetically inhibited as an oxidizing agent when dissolved in water (Brown & Gu, 2006; Mitra and Catalano, 2019). Chlorate has been experimentally shown to oxidize dissolved Fe, and is potent enough to oxidize dissolved Mn, but these experiments show that highly acidic fluids (pH 2) are produced during the reaction (Mitra & Catalano, 2019). Mn oxides are unstable at pH 2, so chlorates as an oxidant are not consistent with current observations (Figure S15 in Supporting Information S1). Bromate has been identified as a possible Mn oxidant (Mitra et al., 2022), but Mn and Br have no correlation in APXS data for these targets (Thompson et al., 2020). The Mitra et al. (2022) results are only relevant to recent acidic groundwater events; the ancient groundwater that altered Murray relevant to this study was most likely alkaline (e.g., Turner et al., 2021). Nitrates may be a candidate for Mn oxidation on Mars or the prebiotic Earth, although Gale crater mudstones have ~10 times less nitrate than those found in Atacama and Antarctic Dry Valley soils (Stern et al., 2015), and the kinetics of these reactions are not currently well-understood (Ranjan et al., 2019). Moreover, photochemical oxidation of Mn with nitrate only occurs in the presence of oxygen in highly alkaline conditions (Jung et al., 2017). Since we do not see major Mn deposits on the Earth until

GOE, and because of the low concentration of nitrate on Mars, nitrate is likely to be ruled out as a key Mn oxidant. Thus, if we rule out UV photolysis, perchlorates, chlorates, bromates, and nitrates as candidates to oxidize Mn, either O_2 was the major oxidant for Mn^{2+} or there are yet unknown processes on Mars that oxidized Mn. Additionally, oxygen as the major oxidant supports the model developed by Hurowitz et al. (2017). Oxygen in the ancient martian atmosphere would need to have a higher abundance than present day Mars O_2 levels (10^{-5} that of present Earth atmospheric O_2; Figure S12 in Supporting Information S1) to oxidize Mn efficiently. This amount of oxygen in the ancient martian atmosphere is difficult to explain using current models (Noda et al., 2019). One recent model suggests that bolide impacts that melted surface ice deposits could episodically increase the O_2 content of the martian atmosphere (Wordsworth et al., 2021). Assuming that these post-impact periods were warm enough to account for the slow process of Mn oxidation, then this scenario may account for some of the Mn oxidation observed in Gale crater (Wordsworth et al., 2021).

5. Conclusions

Observations of Mn-bearing sandstones in Gale crater are consistent with precipitation at the sediment-water interface between anoxic groundwater discharging into shallow lake waters. Our preferred hypothesis is precipitation of Mn oxides along a lake shore where lake water was in equilibrium with an O_2-bearing atmosphere. This scenario of pre-lithification Mn enrichment is supported by the enrichment of Mn in likely more permeable sands versus muds. These observations are further evidence of a long-lived and habitable lake environment in the ancient Gale crater on Mars. How O_2 forms in the Mars atmosphere is currently an open question, though it may be related to bolide impacts. Given the extensive evidence that atmospheric O_2 with biological mediation is the preferred pathway for Mn oxidation on Earth, and the lack of direct evidence for life on Mars, the precipitation of Mn oxides on Mars either points to alkaline (pH > 9) ground or lake water, or a yet unknown mechanism. Excitingly, terrestrial microbial-mediated manganese-rich lake shore deposits have high potential to preserve those organics and biosignatures. In terms of future exploration, we should look for elevated Mn in lake shore deposits that are likely present in Jezero crater's delta (Horgan et al., 2020; Mangold et al., 2021), the landing site for the NASA *Perseverance* rover mission, and if these sediments host enrichments of MnO, they should be prime targets for Mars Sample Return.

Data Availability Statement

All ChemCam spectra (Wiens, 2021a, 2021b), RMIs (Wiens, 2021c, 2021d), Mastcam images (Malin, 2021a), and MAHLI images (Edgett, 2021a, 2021b) used in this work are available from the Planetary Data System (PDS) Geoscience Node (https://pds-geosciences.wustl.edu/missions/msl/chemcam.htm) and the PDS Imaging Node (https://pds-imaging.jpl.nasa.gov/data/mahli/ and https://pds-imaging.jpl.nasa.gov/data/mastcam/). A csv file is provided in this supplement with the chemistry of the individual ChemCam observation points for each target listed in Table 1, and the datapoints plotted in Figure 1 (Gasda et al., 2023).

Acknowledgments
The authors thank JPL for building and operating the *Curiosity* rover as well as the NASA Mars Exploration Program and CNES for their support. P.-Y. Meslin, A. Cousin, S. Maurice, and O. Gasnault acknowledge funding from CNES (Grant 180027). J. Frydenvang acknowledges the support from the Carlsberg Foundation. P. Gasda thanks Kenneth Herkenhoff and Travis Gabriel for useful comments on the manuscript, as well as Bradley Garczynski, Lindsay McHenry, and the anonymous reviewer for their reviews. The authors have no real or perceived financial or other conflicts of interest regarding the publication of this paper. Mastcam mosaics were processed by the Mastcam team at Malin Space Science Systems. Any use of trade, firm, or product names is for descriptive purposes only and does not imply endorsement by the U.S. Government. The research by S. Gwizd was carried out at the Jet Propulsion Laboratory, California Institute of Technology, under a contract with the National Aeronautics and Space Administration (80NM0018D0004).

References

Achilles, C. N., Rampe, E. B., Downs, R. T., Bristow, T. F., Ming, D. W., Morris, R. V., et al. (2020). Evidence for multiple diagenetic episodes in ancient fluvial-lacustrine sedimentary rocks in Gale crater, Mars. *Journal of Geophysical Research: Planets*, *125*(8). https://doi.org/10.1029/2019JE006295

Aller, R. C. (1994). The sedimentary Mn cycle in Long Island Sound: Its role as intermediate oxidant and the influence of bioturbation, O_2, and C_{org} flux on diagenetic reaction balances. *Journal of Marine Research*, *52*(2), 259–295. https://doi.org/10.1357/0022240943077091

Anbar, A. D., & Holland, H. D. (1992). The photochemistry of manganese and the origin of banded iron formations. *Geochimica et Cosmochimica Acta*, *56*(7), 2595–2603. https://doi.org/10.1016/0016-7037(92)90346-K

Arvidson, R. E., Squyres, S. W., Morris, R. V., Knoll, A. H., Gellert, R., Clark, B. C., et al. (2016). High concentrations of manganese and sulfur in deposits on Murray ridge, Endeavour crater, Mars. *American Mineralogist*, *101*(6), 1389–1405. https://doi.org/10.2138/am-2016-5599

Beck, P., Fau, A., Meslin, P.-Y., Forni, O., Lasue, J., Lewin, E., et al. (2017). Searching for carbon on Mars with MSL ChemCam. In *Presented at the 48th lunar and planetary science conference*.

Berger, J. A., Gellert, R., Boyd, N. I., King, P. L., McCraig, M. A., O'Connell-Cooper, C. D., et al. (2020). Elemental composition and chemical evolution of geologic materials in Gale crater, Mars: APXS results from Bradbury landing to the Vera Rubin Ridge. *Journal of Geophysical Research: Planets*, *125*(12), e2020JE006536. https://doi.org/10.1029/2020JE006536

Berger, J. A., King, P. L., Gellert, R., Clark, B. C., Flood, V. A., McCraig, M. A., et al. (2022). Manganese mobility in Gale crater, Mars: Leached bedrock and localized enrichments. *Journal of Geophysical Research: Planets*, *127*(10), e2021JE007171. https://doi.org/10.1029/2021JE007171

Brown, G. M., & Gu, B. (2006). The chemistry of perchlorate in the environment. In B. Gu & J. D. Coates (Eds.), *Perchlorate*. Springer.

Callender, E., & Bowser, C. J. (1976). Freshwater ferromanganese deposits. In K. H. Wolf (Ed.), *Handbook of strata-bound and stratiform ore deposits* (pp. 341–394). Elsevier Scientific Publishing Company.

Calvert, S. E., & Pedersen, T. F. (1996). Sedimentary geochemistry of manganese; implications for the environment of formation of manganiferous black shales. *Economic Geology*, *91*(1), 36–47. https://doi.org/10.2113/gsecongeo.91.1.36

Campbell, J. L., King, P. L., Burkemper, L., Berger, J. A., Gellert, R., Boyd, N. I., et al. (2014). The Mars Science Laboratory APXS calibration target: Comparison of Martian measurements with the terrestrial calibration. *Nuclear Instruments and Methods in Physics Research Section B: Beam Interactions with Materials and Atoms*, *323*, 49–58. https://doi.org/10.1016/j.nimb.2014.01.011

Cao, F., Flemming, R. L., Moser, D. E., Barker, I. R., & Song, Y. (2018). Mineralogy and Shock effects in martian Breccia NWA 8171 by microXRD and Raman spectroscopy. In *Presented at Goldschmidt, Boston, MA*.

Charette, M. A., Sholkovitz, E. R., & Hansel, C. M. (2005). Trace element cycling in a subterranean Estuary: Part 1. Geochemistry of the permeable sediments. *Geochimica et Cosmochimica Acta*, *69*(8), 2095–2109. https://doi.org/10.1016/j.gca.2004.10.024

Clark, J., Sutter, B., Archer, P. D., Ming, D., Rampe, E., McAdam, A., et al. (2021). A review of Sample analysis at Mars-evolved gas analysis laboratory analog work supporting the presence of perchlorates and chlorates in Gale crater, Mars. *Minerals*, *11*(5), 475. https://doi.org/10.3390/min11050475

Clegg, S. M., Frydenvang, J., Anderson, R. B., Vaniman, D. T., Gasda, P., Forni, O., et al. (2020). Quantitative sulfur chemistry observed on diverse samples from sols 1800–2300. In *In the 51st lunar and planetary science conference*.

Clegg, S. M., Wiens, R. C., Anderson, R., Forni, O., Frydenvang, J., Lasue, J., et al. (2017). Recalibration of the Mars Science Laboratory ChemCam instrument with an expanded geochemical database. *Spectrochimica Acta Part B: Atomic Spectroscopy*, *129*, 64–85. https://doi.org/10.1016/j.sab.2016.12.003

Colombera, L., & Mountney, N. P. (2019). The lithofacies organization of fluvial channel deposits: A meta-analysis of modern rivers. *Sedimentary Geology*, *383*, 16–40. https://doi.org/10.1016/j.sedgeo.2019.01.011

Comellas, J. M., Essunfeld, A., Morris, R., Lanza, N., Gasda, P. J., Delapp, D., et al. (2022). Evidence of multiple fluid events in elevated-Mn ChemCam targets in the Bradbury Rise, Gale crater, Mars. In *Presented at the 53rd lunar and planetary science conference, The Woodlands, TX*.

Cronan, D. S., & Thomas, R. L. (1970). Ferromanganese concretions in Lake Ontario. *Canadian Journal of Earth Science*, *7*(5), 1346–1349. https://doi.org/10.1139/e70-128

Das, D., Gasda, P. J., Wiens, R. C., Berlo, K., Leveille, R. J., Frydenvang, J., et al. (2020). Boron and lithium in calcium sulfate veins: Tracking precipitation of diagenetic materials in Vera Rubin Ridge, Gale crater. *Journal of Geophysical Research: Planets*, *125*(8). https://doi.org/10.1029/2019JE006301

David, G., Cousin, A., Forni, O., Meslin, P.-Y., Dehouck, E., Mangold, N., et al. (2020). Analyses of high-iron sedimentary bedrock and diagenetic features observed with ChemCam at Vera Rubin ridge, Gale crater, Mars: Calibration and characterization. *Journal of Geophysical Research: Planets*, *125*(10). https://doi.org/10.1029/2019JE006314

Daye, M., Klepac-Ceraj, V., Pajusalu, M., Rowland, S., Farrell-Sherman, A., Beukes, N., et al. (2019). Light-driven anaerobic microbial oxidation of manganese. *Nature*, *579*(7786), 311–314. https://doi.org/10.1038/s41586-019-1804-0

Dean, W. E., Neff, B. P., Rosenberry, D. O., Winter, T. C., & Parkhurst, R. (2006). The significance of ground water to the accumulation of iron and manganese in the sediments of two hydrologically distinct lakes in north-central Minnesota: A geological perspective. *Groundwater*, *41*(7), 951–963. https://doi.org/10.1111/j.1745-6584.2003.tb02437.x

Edgar, L. A., Fedo, C. M., Gupta, S., Banham, S. G., Fraeman, A. A., Grotzinger, J. P., et al. (2020). A lacustrine paleoenvironment recorded at Vera Rubin ridge, Gale crater: Overview of the sedimentology and stratigraphy observed by the Mars Science Laboratory curiosity rover. *Journal of Geophysical Research: Planets*, *125*(3). https://doi.org/10.1029/2019JE006307

Edgett, K. S. (2021a). MSL mars hand lens imager 4 RDR image V1.0 [Dataset]. *NASA Planetary Data System*. https://doi.org/10.17189/1520292

Edgett, K. S. (2021b). MSL mars hand lens imager 4 RDR ZSTACK V1.0 [Dataset]. *NASA Planetary Data System*. https://doi.org/10.17189/1520169

Edgett, K. S., Caplinger, M. A., Maki, J. N., Ravine, M. A., Ghaemi, F. T., McNair, S., et al. (2015). Curiosity's robotic arm-mounted Mars Hand Lens Imager (MAHLI): Characterization and calibration status: MSL MAHLI technical report, v. 0001. version 2. https://doi.org/10.13140/RG.2.1.3798.5447

Edgett, K. S., Yingst, R. A., Ravine, M. A., Caplinger, M. A., Maki, J. N., Ghaemi, F. T., et al. (2012). Curiosity's Mars Hand Lens Imager (MAHLI) investigation. *Space Science Reviews*, *170*(1–4), 259–317. https://doi.org/10.1007/s11214-012-9910-4

Fedo, C. M., Grotzinger, J., Gupta, S., Stein, N. T., Watkins, J., Banham, S., et al. (2017). Facies analysis and basin architecture of the upper part of the Murray formation, Gale crater, Mars. In *Presented at the 48th lunar and planetary science conference, The Woodlands, TX*.

Fedo, C. M., Grotzinger, J. P., Gupta, S., Fraeman, A., Edgar, L., Edgett, K., et al. (2018). Sedimentology and stratigraphy of the Murray formation, Gale crater, Mars. In *Presented at the 49th lunar and planetary science conference, the Woodlands, TX*.

Force, E. R., & Maynard, J. B. (1991). Manganese: Syngenetic deposits on the margins of anoxic basins. In *Sedimentary and diagenetic mineral deposits: A basin analysis approach to exploration*. Society of Economic Geologists.

Fraeman, A. A., Ehlmann, B. L., Arvidson, R. E., Edwards, C. S., Grotzinger, J. P., Milliken, R. E., et al. (2016). The stratigraphy and evolution of lower Mount Sharp from spectral, morphological, and thermophysical orbital data sets: Stratigraphy and Evolution of Mount Sharp. *Journal of Geophysical Research: Planets*, *121*(9), 1713–1736. https://doi.org/10.1002/2016JE005095

Frakes, L. A., & Bolton, B. R. (1984). Origin of manganese giants: Sea-level change and anoxic-oxic history. *Geology*, *12*(2), 83–86. https://doi.org/10.1130/0091-7613(1984)12<83:oomgsc>2.0.co;2

Froelich, P. N., Klinkhammer, G. P., Bender, M. L., Luedtke, N. A., Heath, G. R., Cullen, D., et al. (1979). Early oxidation of organic matter in pelagic sediments of the eastern equatorial Atlantic: Suboxic diagenesis. *Geochimica et Cosmochimica Acta*, *43*(7), 1075–1090. https://doi.org/10.1016/0016-7037(79)90095-4

Frydenvang, J., Gasda, P. J., Hurowitz, J. A., Grotzinger, J. P., Wiens, R. C., Newsom, H. E., et al. (2017). Diagenetic silica enrichment and late-stage groundwater activity in Gale crater, Mars: Silica enriching diagenesis, Gale, Mars. *Geophysical Research Letters*, *44*(10), 4716–4724. https://doi.org/10.1002/2017GL073323

Frydenvang, J., Mangold, N., Wiens, R. C., Fraeman, A. A., Edgar, L. A., Fedo, C., et al. (2020). The chemostratigraphy of the Murray formation and role of diagenesis at Vera Rubin ridge in Gale crater, Mars, as observed by the ChemCam instrument. *Journal of Geophysical Research: Planets*, *125*(9). https://doi.org/10.1029/2019JE006320

Gasda, P., Lanza, N., Meslin, P.-Y., Lamm, S., Cousin, A., Anderson, R., et al. (2023). Dataset for the manuscript Manganese-rich sandstones as an indicator of ancient oxic lake water conditions in Gale crater, Mars [Dataset]. *Zenodo*. https://doi.org/10.5281/zenodo.7964194

Gasda, P. J., Anderson, R. B., Cousin, A., Forni, O., Clegg, S. M., Ollila, A., et al. (2021). Quantification of manganese for ChemCam Mars and laboratory spectra using a multivariate model. *Spectrochimica Acta Part B: Atomic Spectroscopy*, *181*, 106223. https://doi.org/10.1016/j.sab.2021.106223

Gasda, P. J., Comellas, J., Essunfeld, A., Das, D., Bryk, A. B., Dehouck, E., et al. (2022). Overview of the morphology and chemistry of diagenetic features in the clay-rich Glen Torridon unit of Gale crater, Mars. *Journal of Geophysical Research: Planets*, *127*(12). https://doi.org/10.1029/2021JE007097

Gasda, P. J., Haldeman, E. B., Wiens, R. C., Rapin, W., Bristow, T. F., Bridges, J. C., et al. (2017). In situ detection of boron by ChemCam on Mars: First detection of Boron on Mars. *Geophysical Research Letters*, *44*(17), 8739–8748. https://doi.org/10.1002/2017GL074480

Gorham, E., & Swaine, D. J. (1965). Influence of oxidizing and reducing conditions upon the distribution of some elements in lake sediments. *Limnology & Oceanography*, *10*(2), 268–278.

Grotzinger, J. P., Gupta, S., Malin, M. C., Rubin, D. M., Schieber, J., Siebach, K., et al. (2015). Deposition, exhumation, and paleoclimate of an ancient lake deposit, Gale crater, Mars. *Science*, *350*(6257), aac7575. https://doi.org/10.1126/science.aac7575

Grotzinger, J. P., Sumner, D. Y., Kah, L. C., Stack, K., Gupta, S., Edgar, L., et al. (2014). A habitable fluvio-lacustrine environment at Yellowknife Bay, Gale crater, Mars. *Science*, *343*(6169), 1242777. https://doi.org/10.1126/science.1242777

Gwizd, S., Fedo, C., Grotzinger, J., Banham, S., Rivera-Hernández, F., Stack, K. M., et al. (2022). Sedimentological and geochemical perspectives on a marginal lake environment recorded in the Hartmann's Valley and Karasburg members of the Murray formation, Gale crater, Mars. *Journal of Geophysical Research: Planets*, *127*(8). https://doi.org/10.1029/2022JE007280

Gwizd, S., Fedo, C., Grotzinger, J., Banham, S., Rivera-Hernández, F., Stack, K. M., et al. (2023). Evolution of a lake margin recorded in the Sutton Island member of the Murray formation, Gale crater, Mars. *Journal of Geophysical Research: Planets*, *129*(1). https://doi.org/10.1029/2023JE007919

Gwizd, S., Fedo, C., Grotzinger, J., Edgett, K., Gupta, S., Stack, K. M., et al. (2019). Toward a greater understanding of cross-stratified facies in the Hartmann's Valley member of the Murray formation, Gale crater, Mars. In *Presented at the ninth international conference on Mars, Pasadena, CA*.

Gwizd, S., Fedo, C., Grotzinger, J., Edgett, K., Rivera-Hernández, F., & Stein, N. (2018). Depositional history of the Hartmann's Valley member, Murray formation, Gale crater, Mars. In *Presented at the 49th lunar and planetary science conference, The Woodlands, TX*.

Hansel, C. M. (2017). Chapter two – Manganese in marine microbiology. In R. K. B. T.-A. Poole (Ed.), *Microbiology of metal ions* (pp. 37–83). Academic Press. https://doi.org/10.1016/bs.ampbs.2017.01.005

Hansel, C. M., Zeiner, C. A., Santelli, C. M., & Webb, S. M. M. (I. I. (2012). Oxidation by an ascomycete fungus is linked to superoxide production during asexual reproduction. *Proceedings of the National Academy of Sciences*, *109*(31), 12621–12625. https://doi.org/10.1073/pnas.1203885109

Hoke, M. R. T., Hynek, B. M., & Tucker, G. E. (2011). Formation Timescales of large Martian valley networks. *Earth and Planetary Science Letters*, *312*(1–2), 1–12. https://doi.org/10.1016/j.epsl.2011.09.053

Horgan, B. H. N., Anderson, R. B., Dromart, G., Amador, E. S., & Rice, M. S. (2020). The mineral diversity of Jezero crater: Evidence for possible lacustrine carbonates on Mars. *Icarus*, *339*, 113526. https://doi.org/10.1016/j.icarus.2019.113526

Huckriede, H., & Meischner, D. (1996). Origin and environment of manganese-rich sediments within black-Shale basins. *Geochimica et Cosmochimica Acta*, *60*(8), 1399–1413. https://doi.org/10.1016/0016-7037(96)00008-7

Hurowitz, J. A., Grotzinger, J. P., Fischer, W. W., McLennan, S. M., Milliken, R. E., Stein, N., et al. (2017). Redox stratification of an ancient lake in Gale crater, Mars. *Science*, *356*(6341), eaah6849. https://doi.org/10.1126/science.aah6849

Johnson, J. E., Savalia, P., Davis, R., Kocar, B. D., Webb, S. M., Nealson, K. H., & Fischer, W. W. (2016). Real-time manganese phase dynamics during biological and abiotic manganese oxide reduction. *Environmental Science & Technology*, *50*(8), 4248–4258. https://doi.org/10.1021/acs.est.5b04834

Johnson, J. E., Webb, S. M., Ma, C., & Fischer, W. W. (2016). Manganese mineralogy and diagenesis in the sedimentary rock record. *Geochimica et Cosmochimica Acta*, *173*, 210–231. https://doi.org/10.1016/j.gca.2015.10.027

Johnson, J. E., Webb, S. M., Thomas, K., Ono, S., Kirschvink, J. L., & Fischer, W. W. (2013). Manganese-oxidizing photosynthesis before the rise of cyanobacteria. *Proceedings of the National Academy of Sciences*, *110*(28), 11238–11243. https://doi.org/10.1073/pnas.1305530110

Jones, C., Crowe, S. A., Sturm, A., Leslie, K. L., MacLean, L. C. W., Katsev, S., et al. (2011). Biogeochemistry of manganese in ferruginous lake Matano, Indonesia. *Biogeosciences*, *8*(10), 2977–2991. https://doi.org/10.5194/bg-8-2977-2011

Jung, H., Chadha, T. S., Kim, D., Biswas, P., & Jun, Y.-S. (2017). Photochemically assisted fast abiotic oxidation of manganese and formation of δ-MnO2 nanosheets in nitrate solution. *Chemical Communications*, *53*(32), 4445–4448. https://doi.org/10.1039/C7CC00754J

Kessick, M. A., & Morgan, J. J. (1975). Mechanism of autoxidation of manganese in aqueous solution. *Environmental Science and Technology*, *9*(2), 157–159. https://doi.org/10.1021/es60100a008

Kirschvink, J. L., Gaidos, E. J., Bertani, L. E., Beukes, N. J., Gutzmer, J., Maepa, L. N., & Steinberger, R. E. (2000). Paleoproterozoic snowball Earth: Extreme climatic and geochemical global change and its biological consequences. *Proceedings of the National Academy of Sciences*, *97*(4), 1400–1405. https://doi.org/10.1073/pnas.97.4.1400

Klemm, D. D. (2000). The formation of palaeoproterozoic banded iron formations and their associated Fe and Mn deposits, with reference to the Griqualand West deposits, South Africa. *Journal of African Earth Sciences*, *30*, 1–24. https://doi.org/10.1016/s0899-5362(00)00005-1

Krabbenhoft, D. P., & Anderson, M. P. (1986). Use of a numerical ground-water flow model for hypothesis testing. *Groundwater*, *24*(1), 49–55. https://doi.org/10.1111/j.1745-6584.1986.tb01458.x

Kristensen, E., Kristiansen, K. D., & Jensen, M. H. (2003). Temporal behavior of manganese and iron in a sandy coastal sediment exposed to water column Anoxia. *Estuaries*, *26*(3), 690–699. https://doi.org/10.1007/bf02711980

Kronyak, R. E., Kah, L. C., Edgett, K. S., VanBommel, S. J., Thompson, L. M., Wiens, R. C., et al. (2019). Mineral-filled fractures as indicators of multigenerational fluid flow in the Pahrump Hills member of the Murray formation, Gale crater, Mars. *Earth and Space Science*, *6*(2), 238–265. https://doi.org/10.1029/2018EA000482

Lang, S. C., Payenberg, T. H. D., Reilly, M. R. W., Hicks, T., Benson, J., & Kassan, J. (2004). Modern analogues for dryland sandy fluvial-lacustrine deltas and terminal splay reservoirs. *The APPEA Journal*, *44*(1), 329. https://doi.org/10.1071/AJ03012

Lanza, N. L., Fischer, W. W., Wiens, R. C., Grotzinger, J., Ollila, A. M., Cousin, A., et al. (2014). High manganese concentrations in rocks at Gale crater, Mars. *Geophysical Research Letters*, *41*(16), 5755–5763. https://doi.org/10.1002/2014GL060329

Lanza, N. L., Gasda, P. J., Swanner, E., Fischer, W. W., Treiman, A., Essunfeld, A., et al. (2022). Precipitation of Mn-bearing nodules in a shallow shoreline environment in Gale crater, Mars. In *Presented at the 53rd lunar and planetary science conference, The Woodlands, TX*.

Lanza, N. L., Ollila, A. M., Cousin, A., Wiens, R. C., Clegg, S., Mangold, N., et al. (2015). Understanding the signature of rock coatings in laser-induced breakdown spectroscopy data. *Icarus*, *249*, 62–73. https://doi.org/10.1016/j.icarus.2014.05.038

Lanza, N. L., Wiens, R. C., Arvidson, R. E., Clark, B. C., Fischer, W. W., Gellert, R., et al. (2016). Oxidation of manganese in an ancient aquifer, Kimberley formation, Gale crater, Mars: Manganese fracture fills in Gale crater. *Geophysical Research Letters*, *43*(14), 7398–7407. https://doi.org/10.1002/2016GL069109

Lasue, J., Clegg, S. M., Forni, O., Cousin, A., Wiens, R. C., Lanza, N., et al. (2016). Observation of > 5 wt % zinc at the Kimberley outcrop, Gale crater, Mars. *Journal of Geophysical Research: Planets*, *121*(3), 338–352. https://doi.org/10.1002/2015JE004946

Lasue, J., Cousin, A., Meslin, P.-Y., Mangold, N., Wiens, R. C., Berger, G., et al. (2018). Martian Eolian dust probed by ChemCam. *Geophysical Research Letters*, *45*(20). https://doi.org/10.1029/2018GL079210

Learman, D. R., Voelker, B. M., Vazquez-Rodriguez, A. I., & Hansel, C. M. (2011). Formation of manganese oxides by bacterially generated superoxide. *Nature Geoscience*, *4*(2), 95–98. https://doi.org/10.1038/ngeo1055

Le Mouélic, S., Gasnault, O., Herkenhoff, K. E., Bridges, N. T., Langevin, Y., Mangold, N., et al. (2015). The ChemCam Remote micro-imager at Gale crater: Review of the first year of operations on Mars. *Icarus*, *249*, 93–107. https://doi.org/10.1016/j.icarus.2014.05.030

Lewis, B. L., & Landing, W. M. (1991). The biogeochemistry of manganese and iron in the black Sea. *Deep-Sea Research, Part A: Oceanographic Research Papers*, *38*, S773–S803. Supple (0. https://doi.org/10.1016/s0198-0149(10)80009-3

L'Haridon, J., Mangold, N., Fraeman, A. A., Johnson, J. R., Cousin, A., Rapin, W., et al. (2020). Iron mobility during diagenesis at Vera Rubin ridge, Gale crater, Mars. *Journal of Geophysical Research: Planets*, *125*(11). https://doi.org/10.1029/2019JE006299

L'Haridon, J., Mangold, N., Meslin, P.-Y., Johnson, J. R., Rapin, W., Forni, O., et al. (2018). Chemical variability in mineralized veins observed by ChemCam on the lower slopes of Mount Sharp in Gale crater, Mars. *Icarus*, *311*, 69–86. https://doi.org/10.1016/j.icarus.2018.01.028

Liu, Y., Fischer, W. W., Ma, C., Beckett, J. R., Tschauner, O., Guan, Y., et al. (2021). Manganese oxides in Martian meteorites Northwest Africa (NWA) 7034 and 7533. *Icarus*, *364*, 114471. https://doi.org/10.1016/j.icarus.2021.114471

Liu, Y., Ma, C., Fischer, W. W., Guan, Y., Webb, S. M., Beckett, J. R., et al. (2017). Evidence for O2-rich environments on Mars from hydrous Mn (Iv)-Oxides in Northwest Africa (NWA) 7034 and 7533 meteorites. In *Presented at the 48th lunar and planetary science conference, the Woodlands, TX*.

Malin, M. C. (2021a). MSL mars mast camera 4 RDR image V1.0 [Dataset]. *NASA Planetary Data System*. https://doi.org/10.17189/1520328

Malin, M. C. (2021b). MSL mars mast camera 2 EDR image V1.0 [Dataset]. *NASA Planetary Data System*. https://doi.org/10.17189/1520190

Malin, M. C., & Edgett, K. S. (2000). Sedimentary rocks of early Mars. *Science*, *290*(5498), 1927–1937. https://doi.org/10.1126/science.290.5498.1927

Malin, M. C., Caplinger, M. A., Edgett, K. S., Ghaemi, F. T., Ravine, M. A., Schaffner, J. A., et al. (2010). The Mars science laboratory (MSL) mast-mounted cameras (Mastcams) flight instruments. In *Presented at the 41st lunar and planetary science conference, the Woodlands, TX*.

Mangold, N., Gupta, S., Gasnault, O., Dromart, G., Tarnas, J. D., Sholes, S. F., et al. (2021). Perseverance rover reveals an ancient delta-lake system and flood deposits at Jezero crater, Mars. *Science*, *374*(6568), 711–717. https://doi.org/10.1126/science.abl4051

Maurice, S., Wiens, R. C., Saccoccio, M., Barraclough, B., Gasnault, O., Forni, O., et al. (2012). The ChemCam instrument suite on the Mars Science Laboratory (MSL) rover: Science objectives and mast unit description. *Space Science Reviews*, *170*(1–4), 95–166. https://doi.org/10.1007/s11214-012-9912-2

Meslin, P.-Y., Gasda, P., L'Haridon, J., Forni, O., Lanza, N., Lamm, S., et al. (2018). Detection of hydrous manganese and iron oxides with variable phosphorus and magnesium contents in the lacustrine sediments of the Murray formation, Gale, Mars. In *Presented at the 49th lunar and planetary science conference, the Woodlands, TX*.

Milliken, R. E., Grotzinger, J. P., & Thomson, B. J. (2010). Paleoclimate of Mars as captured by the stratigraphic record in Gale crater. *Geophysical Research Letters*, *37*(4). https://doi.org/10.1029/2009GL041870

Mitra, K., & Catalano, J. G. (2019). Chlorate as a potential oxidant on Mars: Rates and products of dissolved Fe(II) oxidation. *Journal of Geophysical Research: Planets*, *124*(11), 2893–2916. https://doi.org/10.1029/2019JE006133

Mitra, K., Moreland, E. L., Ledingham, G. J., & Catalano, J. G. (2022). Formation of manganese oxides on early Mars due to active halogen cycling. *Nature Geoscience*, *16*(2), 133–139. https://doi.org/10.1038/s41561-022-01094-y

Moore, P. A., Jr., & Reddy, K. R. (1994). Role of Eh and pH on phosphorous geochemistry in sediments of lake Okeechobee, Florida. *Journal of Environmental Quality*, *23*(5), 955–964. https://doi.org/10.2134/jeq1994.00472425002300050016x

Mothersill, J. S., & Shegelski, R. J. (1973). The formation of iron and manganese-rich layers in the holocene sediments of Thunder Bay, lake Superior. *Canadian Journal of Earth Sciences*, *10*(4), 571–576. https://doi.org/10.1139/e73-056

Nachon, M., Clegg, S. M., Mangold, N., Schröder, S., Kah, L. C., Dromart, G., et al. (2014). Calcium sulfate veins characterized by ChemCam/Curiosity at Gale crater, Mars. *Journal of Geophysical Research: Planets*, *119*(9), 1991–2016. https://doi.org/10.1002/2013JE004588

Nachon, M., Mangold, N., Forni, O., Kah, L. C., Cousin, A., Wiens, R. C., et al. (2017). Chemistry of diagenetic features analyzed by ChemCam at Pahrump Hills, Gale crater, Mars. *Icarus*, *281*, 121–136. https://doi.org/10.1016/j.icarus.2016.08.026

Nakamura, A., Miyahara, M., Suga, H., Yamaguchi, A., Wakabayashi, D., Yamashita, S., et al. (2023). Mn-precipitates found in a Martian crustal rock. *Journal of Geophysical Research: Planets*, *128*(9), e2023JE007951. https://doi.org/10.1029/2023JE007951

Nellessen, M. A., Baker, A. M., Newsom, H. E., Jackson, R. S., Williams, J., Nachon, M., et al. (2019). Distribution and analysis of calcium sulfate-cemented sandstones along the MSL traverse, Gale crater, Mars. In *Presented at the 50th lunar and planetary science conference, The Woodlands, TX*.

Noda, N., Imamura, S., Sekine, Y., Kurisu, M., Fukushi, K., Terada, N., et al. (2019). Highly oxidizing aqueous environments on early Mars inferred from scavenging pattern of trace metals on manganese oxides. *Journal of Geophysical Research: Planets*, *124*(5), 1282–1295. https://doi.org/10.1029/2018JE005892

Ostrander, C. M., Nielsen, S. G., Owens, J. D., Kendall, B., Gordon, G. W., Romaniello, S. J., & Anbar, A. D. (2019). Fully oxygenated water columns over continental shelves before the Great Oxidation Event. *Nature Geoscience*, *12*(3), 186–191. https://doi.org/10.1038/s41561-019-0309-7

Ranjan, S., Todd, Z. R., Rimmer, P. B., Sasselov, D. D., & Babbin, A. R. (2019). Nitrogen oxide concentrations in natural waters on early Earth. *Geochemistry, Geophysics, Geosystems*, *20*(4), 2021–2039. https://doi.org/10.1029/2018GC008082

Rapin, W., Ehlmann, B. L., Dromart, G., Schieber, J., Thomas, N. H., Fischer, W. W., et al. (2019). An interval of high salinity in ancient Gale crater lake on Mars. *Nature Geoscience*, *12*(11), 889–895. https://doi.org/10.1038/s41561-019-0458-8

Rapin, W., Meslin, P.-Y., Maurice, S., Vaniman, D., Nachon, M., Mangold, N., et al. (2016). Hydration state of calcium sulfates in Gale crater, Mars: Identification of bassanite veins. *Earth and Planetary Science Letters*, *452*, 197–205. https://doi.org/10.1016/j.epsl.2016.07.045

Rivera-Hernández, F., Sumner, D. Y., Mangold, N., Banham, S. G., Edgett, K. S., Fedo, C. M., et al. (2020). Grain size variations in the Murray formation: Stratigraphic evidence for changing depositional environments in Gale crater, Mars. *Journal of Geophysical Research: Planets*, *125*(2). https://doi.org/10.1029/2019JE006230

Rivera-Hernández, F., Sumner, D. Y., Mangold, N., Stack, K. M., Forni, O., Newsom, H., et al. (2019). Using ChemCam LIBS data to constrain grain size in rocks on Mars: Proof of concept and application to rocks at Yellowknife Bay and Pahrump Hills, Gale crater. *Icarus*, *321*, 82–98. https://doi.org/10.1016/j.icarus.2018.10.023

Rossmann, R., & Callender, E. (1968). Manganese nodules in Lake Michigan. *Science*, *162*(3858), 1123–1124. https://doi.org/10.1126/science.162.3858.1123

Rossmann, R., & Callender, E. (1969). Geochemistry of Lake Michigan manganese nodules. In *Proceedings – Twelfth conference on Great lakes research, held at the University of Michigan, Ann Arbor, May 5–7 1969* (pp. 306–316).
Schissel, D., & Aro, P. (1992). The major early Proterozoic sedimentary iron and manganese deposits and their tectonic setting. *Economic Geology*, *87*(5), 1367–1374. https://doi.org/10.2113/gsecongeo.87.5.1367
Schmidt, M. E., Perrett, G. M., Bray, S. L., Bradley, N. J., Lee, R. E., Berger, J. A., et al. (2018). Dusty rocks in Gale crater: Assessing areal coverage and separating dust and rock contributions in APXS analyses. *Journal of Geophysical Research: Planets*, *123*(7), 1649–1673. https://doi.org/10.1029/2018JE005553
Schwenzer, S. P., Abramov, O., Allen, C. C., Bridges, J. C., Clifford, S. M., Filiberto, J., et al. (2012). Gale Crater: Formation and post-impact hydrous environments. *Planetary and Space Science*, *70*(1), 84–95. https://doi.org/10.1016/j.pss.2012.05.014
Schwenzer, S. P., Bridges, J. C., Wiens, R. C., Conrad, P. G., Kelley, S. P., Leveille, R., et al. (2016). Fluids during diagenesis and sulfate vein formation in sediments at Gale crater, Mars. *Meteoritics & Planetary Science*, *51*(11), 2175–2202. https://doi.org/10.1111/maps.12668
Siebach, K. L., Grotzinger, J. P., Kah, L. C., Stack, K. M., Malin, M., Léveillé, R., & Sumner, D. Y. (2014). Subaqueous shrinkage cracks in the Sheepbed mudstone: Implications for early fluid diagenesis, Gale crater, Mars. *Journal of Geophysical Research: Planets*, *119*(7), 1597–1613. https://doi.org/10.1002/2014JE004623
Stack, K. M., Grotzinger, J. P., Lamb, M. P., Gupta, S., Rubin, D. M., Kah, L. C., et al. (2019). Evidence for plunging river plume deposits in the Pahrump Hills member of the Murray formation, Gale crater, Mars. *Sedimentology*, *66*(5), 1768–1802. https://doi.org/10.1111/sed.12558
Stein, N., Grotzinger, J. P., Schieber, J., Mangold, N., Hallet, B., Newsom, H., et al. (2018). Desiccation cracks provide evidence of lake drying on Mars, Sutton Island member, Murray formation, Gale crater. *Geology*, *46*(6), 515–518. https://doi.org/10.1130/G40005.1
Stern, J. C., Sutter, B., Freissinet, C., Navarro-González, R., McKay, C. P., Archer, P. D., et al. (2015). Evidence for indigenous nitrogen in sedimentary and aeolian deposits from the Curiosity rover investigations at Gale crater, Mars. *Proceedings of the National Academy of Sciences*, *112*(14), 4245–4250. https://doi.org/10.1073/pnas.1420932112
Stumm, W., & Morgan, J. J. (1996). *Aquatic chemistry: Chemical equilibria and rates in natural waters* (3rd ed., p. 1042). John Wiley.
Sun, V. Z., Stack, K. M., Kah, L. C., Thompson, L., Fischer, W., Williams, A. J., et al. (2019). Late-stage diagenetic concretions in the Murray formation, Gale crater, Mars. *Icarus*, *321*, 866–890. https://doi.org/10.1016/j.icarus.2018.12.030
Tebo, B. M., Bargar, J. R., Clement, B. G., Dick, G. J., Murray, K. J., Parker, D., et al. (2004). Biogenic manganese oxides: Properties and mechanisms of formation. *Annual Reviews in Earth Planetary Sciences*, *32*(1), 287–328. https://doi.org/10.1146/annurev.earth.32.101802.120213
Tebo, B. M., Nealson, K. H., Emerson, S., & Jacobs, L. (1984). Microbial mediation of Mn(II) and Co(II) precipitation at the O_2/H_2S interfaces in two anoxic Fjords. *Limnology & Oceanography*, *29*(6), 1247–1258. https://doi.org/10.4319/lo.1984.29.6.1247
Thomas, N. H., Ehlmann, B. L., Meslin, P.-Y., Rapin, W., Anderson, D. E., Rivera-Hernández, F., et al. (2019). Mars science laboratory observations of chloride salts in Gale crater, Mars. *Geophysical Research Letters*, *46*(19), 10754–10763. https://doi.org/10.1029/2019GL082764
Thomas, N. H., Ehlmann, B. L., Rapin, W., Rivera-Hernández, F., Stein, N. T., Frydenvang, J., et al. (2020). Hydrogen variability in the Murray Formation, Gale crater, Mars. *Journal of Geophysical Research: Planets*, *125*(9). https://doi.org/10.1029/2019JE006289
Thompson, L. M., Berger, J. A., Spray, J. G., Fraeman, A. A., McCraig, M. A., O'Connell-Cooper, C. D., et al. (2020). APXS-Derived compositional characteristics of Vera Rubin Ridge and Murray formation, Gale crater, Mars: Geochemical implications for the origin of the ridge. *Journal of Geophysical Research: Planets*, *125*(10). https://doi.org/10.1029/2019JE006319
Thorpe, M. T., Bristow, T. F., Rampe, E. B., Tosca, N. J., Grotzinger, J. P., Bennett, K. A., et al. (2022). Mars science laboratory CheMin data from the glen Torridon region and the significance of lake-groundwater interactions in interpreting mineralogy and sedimentary history. *Journal of Geophysical Research: Planets*, *127*(11). https://doi.org/10.1029/2021JE007099
Treiman, A. H., Lanza, N. L., VanBommel, S., Berger, J., Wiens, R., Bristow, T., et al. (2023). Manganese-iron phosphate nodules at the Groken site, Gale crater, Mars. *Minerals*, *13*(9), 1122. https://doi.org/10.3390/min13091122
Tsikos, H., Beukes, N. J., Moore, J. M., & Harris, C. (2003). Deposition, diagenesis, and secondary enrichment of metals inthe paleoproterozoic hotazel iron formation, kalahari manganese field, South Africa. *Economic Geology*, *98*(7), 1449–1462. https://doi.org/10.2113/gsecongeo.98.7.1449
Turner, S. M. R., Schwenzer, S. P., Bridges, J. C., Rampe, E. B., Bedford, C. C., Achilles, C. N., et al. (2021). Early diagenesis at and below Vera Rubin ridge, Gale crater, Mars. *Meteoritics & Planetary Science*, *56*(10), 1905–1932. https://doi.org/10.1111/maps.13748
Vaniman, D. T., Bish, D. L., Ming, D. W., Bristow, T. F., Morris, R. V., Blake, D. F., et al. (2014). Mineralogy of a mudstone at Yellowknife Bay, Gale crater, Mars. *Science*, *343*(6169), 1243480. https://doi.org/10.1126/science.1243480
van Waasbergen, L. G., Hildebrand, M., & Tebo, B. M. (1996). Identification and characterization of a gene cluster involved in manganese oxidation by spores of the marine Bacillus Sp. Strain SG-1. *Journal of Bacteriology*, *178*(12), 3517–3530. https://doi.org/10.1128/jb.178.12.3517-3530.1996
Vasavada, A. R. (2022). Mission overview and scientific contributions from the Mars Science Laboratory curiosity rover after eight years of surface operations. *Space Science Reviews*, *218*(3), 14. https://doi.org/10.1007/s11214-022-00882-7
Wentworth, C. K. (1922). A scale of grade and class terms for clastic sediments. *The Journal of Geology*, *30*(5), 377–392. https://doi.org/10.1086/622910
Wiens, R. C., Blazon-Brown, A. J., Melikechi, N., Frydenvang, J., Dehouck, E., Clegg, S. M., et al. (2021). Improving ChemCam LIBS long-distance elemental compositions using empirical abundance trends. *Spectrochimica Acta Part B: Atomic Spectroscopy*, *182*, 106247. https://doi.org/10.1016/j.sab.2021.106247
Wiens, R. C., Maurice, S., Barraclough, B., Saccoccio, M., Barkley, W. C., Bell, J. F. I. I. I., et al. (2012). The ChemCam instrument suite on the Mars Science Laboratory (MSL) rover: Body unit and combined system tests. *Space Science Reviews*, *170*(1–4), 167–227. https://doi.org/10.1007/s11214-012-9902-4
Wiens, R. C., Maurice, S., Lasue, J., Forni, O., Anderson, R. B., Clegg, S., et al. (2013). Pre-flight calibration and initial data processing for the ChemCam laser-induced breakdown spectroscopy instrument on the Mars Science Laboratory rover. *Spectrochimica Acta Part B: Atomic Spectroscopy*, *82*, 1–27. https://doi.org/10.1016/j.sab.2013.02.003
Wiens, R. (2021a). MSL chemcam laser induced breakdown spectrometer EDR V1.0 [Dataset]. *NASA Planetary Data System*. https://doi.org/10.17189/1519439
Wiens, R. (2021b). MSL mars chemcam LIBS spectra 4/5 RDR V1.0 [Dataset]. *NASA Planetary Data System*. https://doi.org/10.17189/1519485
Wiens, R. (2021c). MSL chemcam remote micro imaging camera EDR V1.0 [Dataset]. *NASA Planetary Data System*. https://doi.org/10.17189/1519456
Wiens, R. (2021d). MSL mars chemcam remote micro-imager camera 5 RDR V1.0 [Dataset]. *NASA Planetary Data System*. https://doi.org/10.17189/1519494

Wordsworth, R., Knoll, A. H., Hurowitz, J., Baum, M., Ehlmann, B. L., Head, J. W., & Steakley, K. (2021). A coupled model of episodic warming, oxidation and geochemical transitions on early Mars. *Nature Geoscience*, *14*(3), 127–132. https://doi.org/10.1038/s41561-021-00701-8

Yao, W., & Millero, F. J. (1996). Adsorption of phosphate on manganese dioxide in seawater. *Environmental Science & Technology*, *30*(2), 536–541. https://doi.org/10.1021/es950290x

Yen, A. S., Ming, D. W., Vaniman, D. T., Gellert, R., Blake, D. F., Morris, R. V., et al. (2017). Multiple stages of aqueous alteration along fractures in mudstone and sandstone strata in Gale Crater, Mars. *Earth and Planetary Science Letters*, *471*, 186–198. https://doi.org/10.1016/j.epsl.2017.04.033

Yu, H., & Leadbetter, J. R. (2020). Bacterial chemolithoautotrophy via manganese oxidation. *Nature*, *583*(7816), 453–458. https://doi.org/10.1038/s41586-020-2468-5

Zavala, C., & Pan, S. (2018). Hyperpycnal flows and hyperpycnites: Origin and distinctive characteristics. *Lithologic Reservoirs*, *30*(1), 1–27. https://doi.org/10.3969/j.issn.1673-8926.2018.01.001

References From the Supporting Information

Meslin, P.-Y., Gasnault, O., Forni, O., Schroder, S., Cousin, A., Berger, G., et al. (2013). Soil diversity and hydration as observed by ChemCam at Gale crater, Mars. *Science*, *341*(6153), 1238670. https://doi.org/10.1126/science.1238670